A Window into Early Middle Paleolithic Human Occupational Layers: Misliya Cave, Mount Carmel, Israel

MINA WEINSTEIN-EVRON
Zinman Institute of Archaeology, University of Haifa, Mount Carmel, Haifa 31905, ISRAEL; evron@research.haifa.ac.il

ALEXANDER TSATSKIN
Zinman Institute of Archaeology, University of Haifa, Mount Carmel, Haifa 31905, ISRAEL; tsatskin@research.haifa.ac.il

STEPHEN WEINER
Kimmel Center for Archaeological Science, Weizmann Institute of Science, Rehovot 76100, ISRAEL; steve.weiner@weizmann.ac.il

RUTH SHAHACK-GROSS
Kimmel Center for Archaeological Science, Weizmann Institute of Science, Rehovot 76100, ISRAEL; ruth.shahack@weizmann.ac.il

AMOS FRUMKIN
Geography Department, The Hebrew University, Jerusalem 91905, ISRAEL; msamos@mscc.huji.ac.il

REUVEN YESHURUN
Zinman Institute of Archaeology, University of Haifa, Mount Carmel, Haifa 31905, ISRAEL; ryeshuru@research.haifa.ac.il

YOSSI ZAIDNER
Zinman Institute of Archaeology, University of Haifa, Mount Carmel, Haifa 31905, ISRAEL; yzaidner@research.haifa.ac.il

ABSTRACT

Misliya Cave, Mount Carmel, Israel, contains rich Early Middle Paleolithic (EMP) habitation layers. Sediments within a deep 1m² sounding at the Upper Terrace of the site underwent detailed geoarchaeological analyses, coupled with techno-typological and taphonomic analyses of the archaeological material that enabled a focused look deep into the layers. While no significant temporal changes were observed in the lithic or faunal assemblages that for the most part represent EMP occupations, the caves' configuration underwent major changes. The EMP sequence was deposited under the cave roof whose westward extension retreated gradually. We distinguished two main sedimentological cycles and possibly also occupational phases above either a massive rockfall or bedrock, separated by a gap of undetermined duration that was, however, long enough to have created a distinct paleosurface. These cycles are related to major phases of cave collapse and it was only after the roof had fully fallen that the upper deposits were cemented as a result of rain water and exposure to the elements. Exceptional preservation of laminated vegetal tissues, found in the earlier cycle before the cave's roof collapse, is associated with wood ash, burnt bones, and phytoliths. We tentatively suggest that this association constitutes the earliest evidence to date for bedding or matting.

INTRODUCTION

The Middle Paleolithic in the Levant covers a time-span of roughly 200,000 years (ca. 250–50 ka BP; Mercier et al. 2007; Mercier and Valladas 2003; Rink et al. 2001; Schwarcz and Rink 1998; Schwarcz et al. 1989; Valladas et al. 1987, 1999). This long period is commonly divided into three chronologically and culturally defined facies (Copeland 1975; Meignen and Bar-Yosef 1992; Bar-Yosef 1998). The earliest Middle Paleolithic industries known as Early Levantine Mousterian, or according to the Tabun Cave type section, Mousterian of Tabun D-type, are currently dated to ca. 250–170 ka (ibid, Rink et al. 2003, 2004). These industries are characterized by use of true laminar technology alongside Levallois method (e.g., Meignen 1998, 2011; Wojtczak 2011).

The Early Middle Paleolithic (EMP) still remains one of the less-studied facies of the Levantine Middle Paleolithic, probably because only a few EMP sites have been discovered so far. Hayonim, Tabun, and Misliya caves are the only sites in the Mediterranean zone of the Levant that con-

PaleoAnthropology 2012: 202–228. ISSN 1545-0031
doi:10.4207/PA.2012.ART75

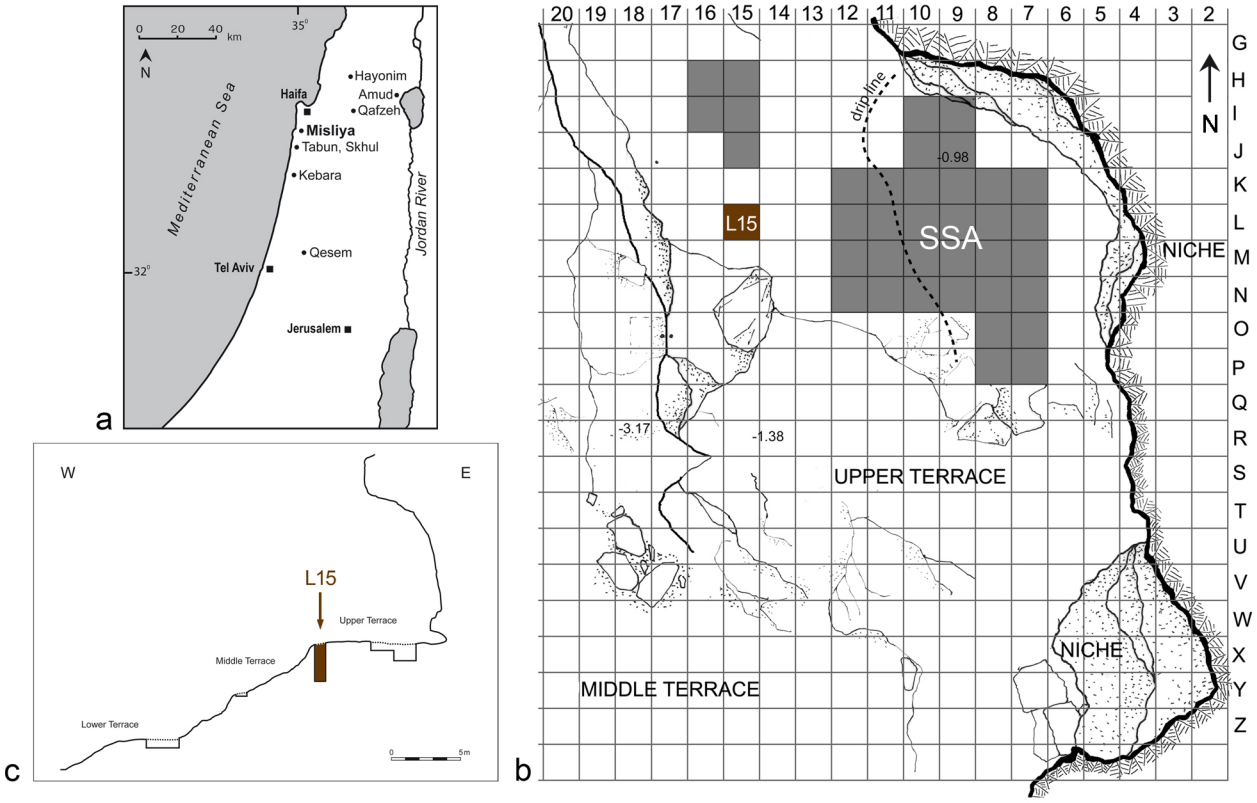

Figure 1. Location map, with main excavated area on the Upper Terrace of Misliya Cave.

tain EMP layers and were explored by modern techniques (Bar-Yosef 1998; Bar-Yosef et al. 2005; Jelinek 1982; Jelinek et al. 1973; Meignen et al. 2006; Weiner et al. 1995, 2002; Weinstein-Evron et al. 2003a). While the two former sites exhibit low occupation intensities suggesting brief, infrequent visits, Misliya Cave was found to contain extensive EMP habitation layers with extremely rich lithic and faunal assemblages pointing to more intensive occupation.

In this paper we present results of excavation along a natural dissolution channel within the cemented layers on the Upper Terrace of Misliya Cave which enables a focused look deep into the layers. This enables tracking temporal changes within the lithic and faunal assemblages, better understanding of the human use of this part of the site, reconstructing possible changes in cave configuration through time, and establishing when the cave reached its present-day form. We first provide a general description of the site in its wider geological setting followed by a close-up look into the stratigraphy and archaeological content of the deepest sounding at the site. Detailed geoarchaeological analyses will then be used to decipher possible stages in the collapse of the cave's ceiling and changes in the cave's configuration during the EMP occupation of the site, as apparent in the sounding.

BACKGROUND

Misliya Cave is located on the western slopes of Mount Carmel, slightly to the south of Nahal (Wadi) Sefunim ($32^{0}45'$N, $34^{0}58'$E; Israel grid), at an elevation of ca. 90masl, some 12km south of Haifa (Figure 1). Situated 7km north of Nahal Me'arot (Wadi el-Mughara) and the caves of Tabun, Jamal, el-Wad, and Shkul (Garrod and Bate 1937; Jelinek et al. 1973; McCown 1937; Weinstein-Evron and Tsatskin 1994, 1995; Zaidner et al. 2005), the cave was found to contain rich Middle Paleolithic (Mousterian) and Lower Paleolithic (Acheulo-Yabrudian) layers (Weinstein-Evron et al. 2003a; Zaidner et al. 2006).

Today the site appears as a rock shelter or an overhang (Figure 2), carved into the limestone cliff. However, its form, together with remnants of enclosing walls, the ancient flowstones, and the numerous boulders within the brecciated layers and along the slope, suggests that it is a large collapsed cave. The cliff at Misliya, facing W/SW, is composed of alternating layers of limestone, about 1–2m thick, of variable texture and hardness. Strongly cemented archaeological sediments (breccia) are found on three terrace-like surfaces at the base of the cliff, all sloping gently to the west (henceforth Upper, Middle, and Lower Terraces; see Figures 1, 2). Sub-vertical exposures between the terraces were formed in the course of natural collapse of the cave, and cementation and erosion of its deposits. The surface of the Lower Terrace is located about 10m below that of the Upper Terrace. In the eastern part of the Upper Terrace, roughly below the present drip-line, cemented layers change laterally into softer sediments, forming an area of about $20m^2$, designated as the "Soft Sediments Area" (SSA; see Figure 1). This area, in contrast with the cemented sediments, is more amenable to excavation, and lithics and animal bones can be extracted from its sediments without the risk of being broken; it was the focus of excavation. A series

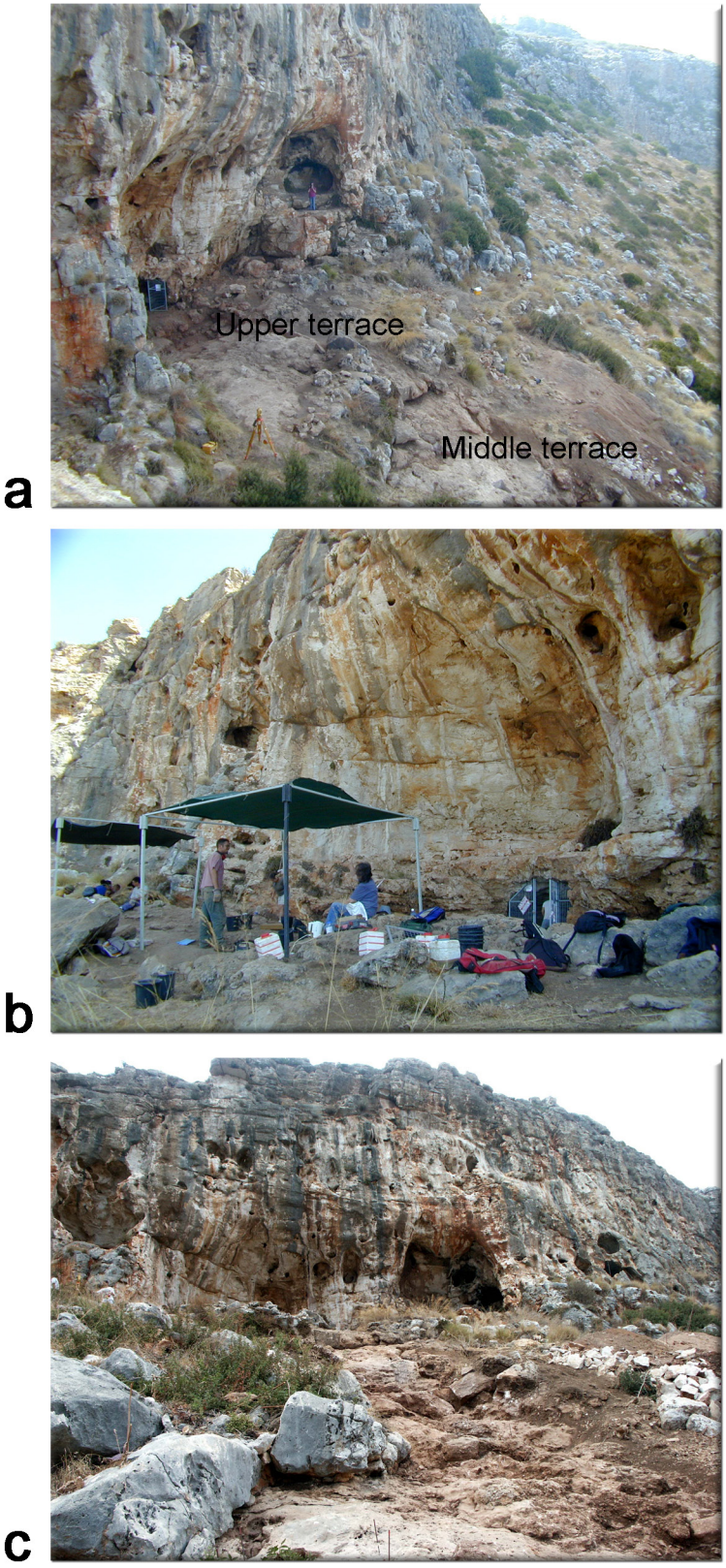

Figure 2. The collapsed Misliya Cave. (a) a view to the south of the excavated area, from the top of the cliff; (b) the rock overhang above the main excavation area; note the rounded form and the smooth walls of a former, now mostly collapsed cave; (c) a view from the west.

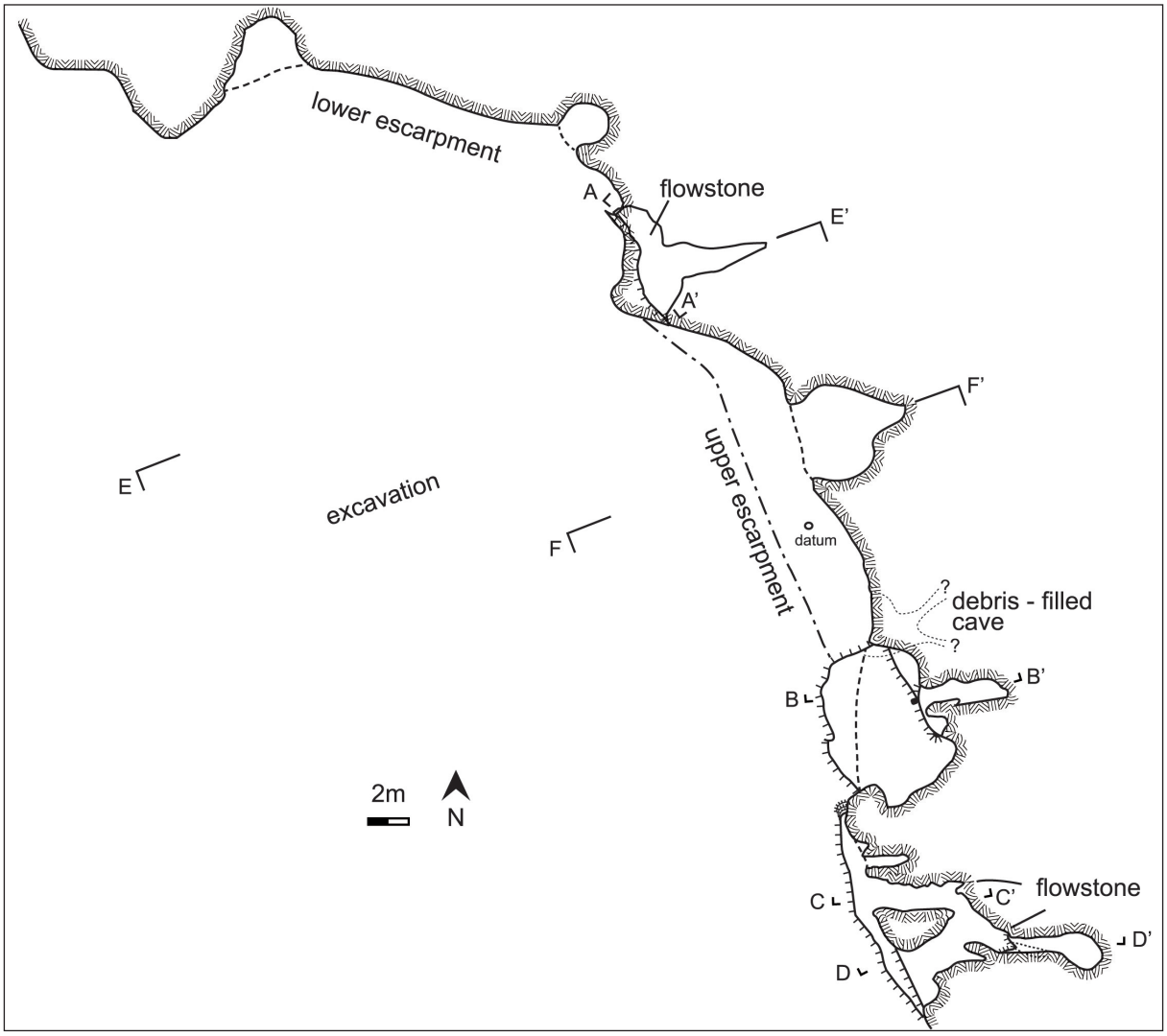

Figure 3. The Misliya cliff, with location of topographic features, caves, and flowstones.

of well-preserved hearths constitutes the main feature of this area. The sounding in Square L15, two meters west of the SSA (see Figure 1), provides the deepest section at the site and hence was chosen for illuminating the sequence of EMP habitations at Misliya Cave.

GEOLOGY

Mount Carmel is located along the northern coast of Israel and reaches a maximum altitude of 540m. Its lithology is composed of Cretaceous carbonate rocks—limestones, dolomites, chalks, and marls (Karcz 1958; Segev and Sass 2009a, b), as well as volcanics. The area is intensively dissected by faults, fractures, and joints, with well-developed karstic features and numerous caves mainly along the western escarpment and some of the wadis running west.

At Misliya, the western escarpment of Mount Carmel is composed of Turonian bioclastic limestone of the lower part of the Bi'na Formation, Muhraqa Member, dated to 95–93 Ma (Segev and Sass 2009a). The bedrock is characterized by massive, almost horizontal layers of indurated reef deposit, with abundant fossils and few fractures. The later uplift of the Carmel ridge resulted in karst dissolution and cave formation (Segev and Sass 2009a).

The studied part of the escarpment, where the site is located, is ~60m long (Figure 3) and ~12–15m high (17–20m high at its highest part) (Figure 4, sections EE' and FF'), towering above the site. The cliff includes a rock shelter 15m long, under a rock overhang, which may have been originally part of a large cave chamber (see Figure 2). Several small caves (or niches) extend eastward from the rock shelter and from the continuation of the cliff northward and southward, up to 10m eastward/inward from the cliff face (see Figure 3).

The morphologic features observed in the caves—smooth walls, tube-like passages with elliptical cross section, ceiling cupolas, and a combination of elongated passages with larger chambers indicate that the overhang is a remnant of a collapsed cave or cave system. An ancient, inactive, flowstone appears in the southern and northern caves (see Figure 4; sections AA', CC', DD', EE'). It forms a 0.2–0.5m thick macrocrystalline calcite layer in the southern cave, and two such layers in the northern cave (section

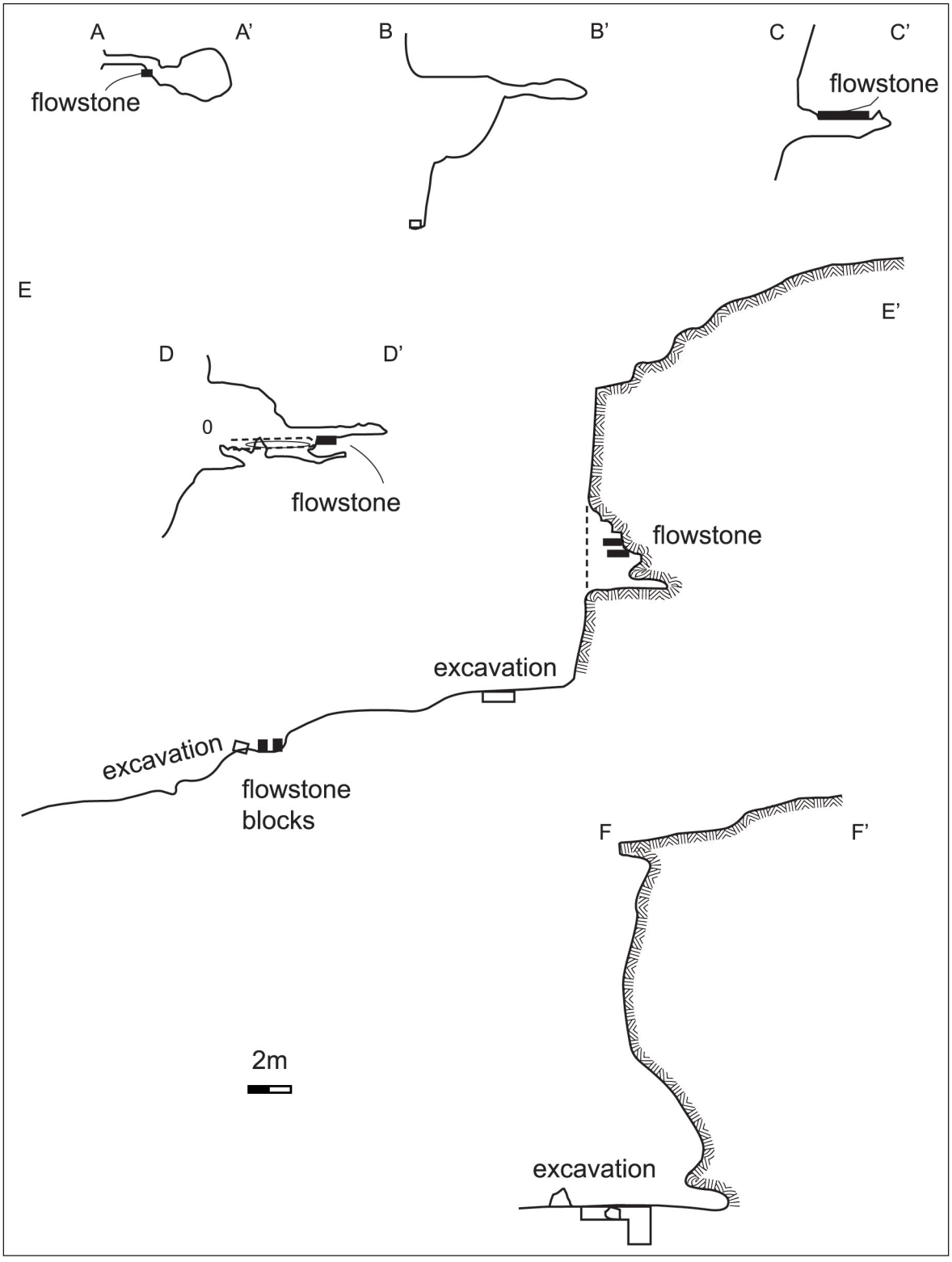

Figure 4. Sections along the Misliya cliff (for location see Figure 3).

EE′). The flowstone is more resistant to erosion than the reef bedrock. Some later expansion of the cave occurred above and below the flowstone, while the flowstone itself was undermined and eroded to a lesser degree. Detached blocks of flowstone appear some 20m west of the cliff within collapsed debris and archaeological cemented sediments (section EE′). Th/U dating of one of these collapsed flowstone blocks on the Lower Terrace shows that it is older than 650 ky (H. Schwarcz, personal communication, 2003). While the date cannot be associated with the archaeological

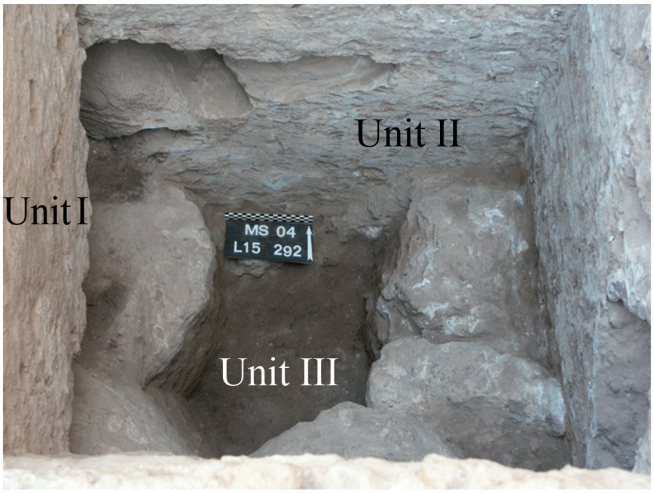

Figure 5. The excavation of the deep section in Square L15.

layers, it indicates that the cave formation was already in process prior to that time. The appearance of the block and its old age indicate that most probably it originated from a former westward extension of the flowstone observed *in situ* in the northern and southern niches. This extension must have formed a part of the cave system, later destroyed by collapse.

THE CHRONOLOGICAL FRAMEWORK

Radiometric dating of the site is still in progress. A single optically stimulated luminescence sample from the top of the brecciated sediments of Square O17 yielded an age of 130±33 ky, considered to be a minimum age due to signal saturation (Weinstein-Evron et al. 2003a). TL dates on burnt MP flint artifacts from various contexts in the Upper Terrace of Misliya Cave range between 250 and 160 ky (Valladas et al. in preparation).

The lithic analysis of the MP assemblages of Misliya Cave (Weinstein-Evron et al. 2003a, and see below) shows that they all belong to the EMP (e.g., Bar-Yosef 1998; Garrod and Bate 1937; Jelinek 1982). The same cultural phase is dated to ca. 250–170 ky BP in both caves and open-air Levantine Middle Paleolithic sites (Grün and Stringer 2000; Mercier and Valladas 2003; Mercier et al. 2007; Rink et al. 2003). Thus the lithic evidence and preliminary radiometric dates seem to be in general agreement with the known record of the Levantine EMP, broadly assigning the site to Marine Isotope Stage (MIS) 7.

THE DEEP SOUNDING OF SQUARE L15

STRATIGRAPHY

Our trial excavation was conducted in Square L15 (see Figure 1), at the western part of the Upper Terrace, in an area where a geophysical survey of the cave indicated the occurrence of the deepest sediments above bedrock (Weinstein-Evron et al. 2003b). As the cemented sediments are extremely hard we excavated by following deep, natural karstic cavities within the lithified layers (Figure 5). While this has resulted in uneven volumes of excavated material along the sequence, it considerably facilitated our excavation and ensured minor loss of archaeological material for any future spatial analysis. The cemented sediments of Square L15 were excavated in 5cm spits by hand-chiseling or with an electrical hammer. In addition to items collected in the field, this procedure produced lumps of cemented sediments which were further excavated in the laboratory for extraction of archaeological material.

The sounding was excavated to a depth of about 3.5m below surface where it reached a massive rock (either bedrock or an ancient rock fall), occupying the bulk of the sounding. The stratigraphic section, presented in Figure 6, shows the northern (N) face of the sounding together with the lower portion of its western (W) face, where the lowermost unit excavated thus far has been unearthed, due to the westward inclination of the underlying rock surface. Four stratigraphic units were defined (from top to bottom) (see Figure 6):

Unit I: 0.75–1.85m, cemented clay loam, calcareous, contains lenses varying from brown-gray to yellowish brown (Munsell YR10 2/6–YR10 4/5), sometimes light yellow (Y2.5 4/8). The lower contact is determined by gradual change to softer deposits.

Unit II: 1.85–2.7/2.95m, light brown (10YR 6/4) cemented clay loam that contains more stones (up to about 30%) of different sizes, from 5cm to 20cm long. The stones are commonly covered by a weathering rim that varies in color from yellowish to blackish and peels easily off the hard core. There are many erosional cavities in the sediments (see Figure 5). The cavities are of ca. 10–40cm in diameter and of strongly convoluted configuration. At the contact with Unit III erosional channels acquire a more or less subhorizontal configuration, whose outlets may be seen several meters westward in the 'cliff' of the Upper Terrace. The lower contact that slopes westwards (see Figure 6) is sharp and defined by color, increase in moisture, and decrease in hardness.

Unit III extends from the bottom contact of Unit II to the large rock surface (rock fall?) at a depth of about 3.75m below datum (on the N wall), and is divided into two subunits:

Sub-unit IIIa is composed of alternating lens-shaped loamy layers, varying in color from black and brown to reddish-brown (5YR 4/4), ranging from 2cm to 5–6cm in thickness. The layers generally slope westwards and show distinct, occasionally distorted outlines. This sub-unit is softer than the upper layers and the lower-lying deposits. Sub-unit IIIb, lying on the large stone at the bottom of the section is characterized by stronger induration. The number of indurated lenses significantly increases in the lower subunit IIIb, where they dip up to 20°. Although the exposed area is limited, dips seem to increase in the western corner of the section, i.e., slope-ward. In addition, the distinct black or dark brown lenses stretch from east to west on longer distances than above. The lower contact is sharp. It was uncovered only in the western wall of the square where there was the possibility of further excavation due to

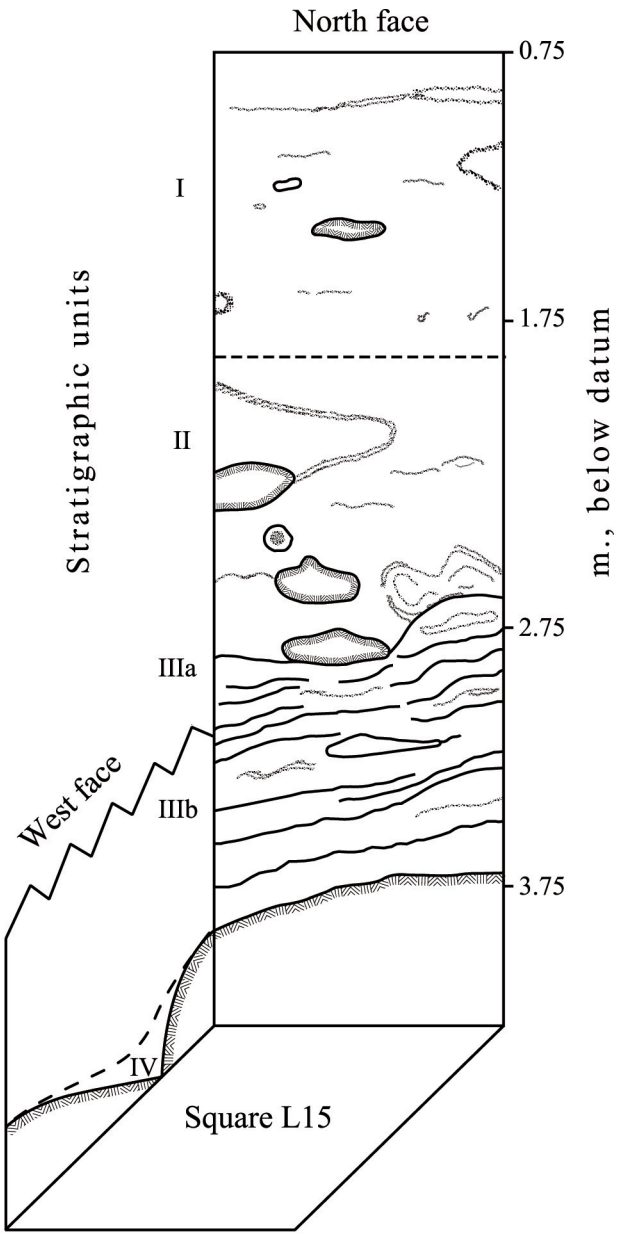

Figure 6. Stratigraphic section of Square L15.

natural sloping of the large rock surface.

Unit IV, 3.75m to 4.0m below datum (the visible depth; in the western section of the sounding only) is composed of hard dark-brown (7.5YR 3/4) loam, probably filling a cavity on the rock surface. The sediments are not as well cemented as those in the upper units.

Although the L15 section was divided in the field into four distinct units, it is worth noting that the nature of each unit is heterogeneous and their deposits all contain abundant black dots, mottles and coatings, albeit in different degrees of preservation and types of occurrence within various units.

GEOARCHAEOLOGY

In order to identify the materials composing the sediments in the L15 section, and to reconstruct the sequence of depositional and post-depositional processes we used micromorphology, SEM/EDS analyses, Fourier Transform Infrared (FTIR) spectroscopy, and phytolith analysis.

Micromorphology

Thin sections were prepared after impregnation of undisturbed blocks by polyester resin under vacuum, analyzed with a polarized light microscope (Olympus BH-2) and described according to Bullock et al. (1985). Both standard (24x36mm) and large-sized (51x75mm) thin sections were analyzed.

Unit I: The deposits of Unit I exhibit a very dense *mélange* of heterogeneous calcareous mass. It contains less than ca. 10% unsorted quartz sand, reddish decalcified and cracked soil aggregates (obviously derived from *terra rossa* from outside the cave, occasionally up to 1.5mm in size; Figure 7a and b), and bone fragments ranging between 0.1-0.5mm in length. In the lower part of Unit I, shells up to 0.5mm long and in various states of preservation and secondary recrystallization are found (e.g., Figure 7c and d). The strong fragmentation of bones resulting in a characteristic microfabric (Figure 8a and b) is probably due to both syn-depositional human activity (i.e., ashes) and post-depositional processes, such as shrink-swell, mechanical attrition (e.g., trampling), and/or secondary calcite crystallization. Occasionally bones are coated with discontinuous and uneven black isotropic lining (Figure 8c and d), whose origin will be discussed below. Charcoal appears to be fragmented into particles of ca. 0.8mm in diameter and less, with no visible cellular structure (Figure 9a). Abundant fractures within charcoal fragments may testify to aging and secondary disruptions due to either secondary crystallization or swell/shrink processes. The charred features are scattered in the sediments without being strictly localized to dark-colored lenses, occasionally recognizable in the field. Lastly, chips of flint, covered with clay, were observed (Figure 9b and c). Taking into account field observations on burnt, shattered flints, it is tentatively suggested that these clay-stained chips were the result of such thermal alteration.

Unit II: The sediments in this unit are associated with increased porosity, incipient lamination, and secondary carbonate deposition. They also contain abundant small and medium-sized angular stones. White-colored sediments within this unit exhibit a dense calcitic microfabric composed of both micritic and microsparitic calcite. It incorporates small fragments of anthropogenic debris, represented by chips of bones (50–100μm) and subrounded clay aggregates (20–40μm) (Figure 10a and b). Less dense patches show the juxtaposition of calcitic and decalcified clay-enriched areas with interplanar voids (less than 10% porosity), partly filled by post-depositional micrite (Figure 11a and b). The occurrence of post-depositional precipitation of microsparitic calcite in elongated pores, apparently from highly concentrated solutions, is evidenced in the form of secondary carbonate patches (Figure 11c). Thin sections from the stones (Figure 12a) that are abundant in Unit II showed a gradual contact between the stones and

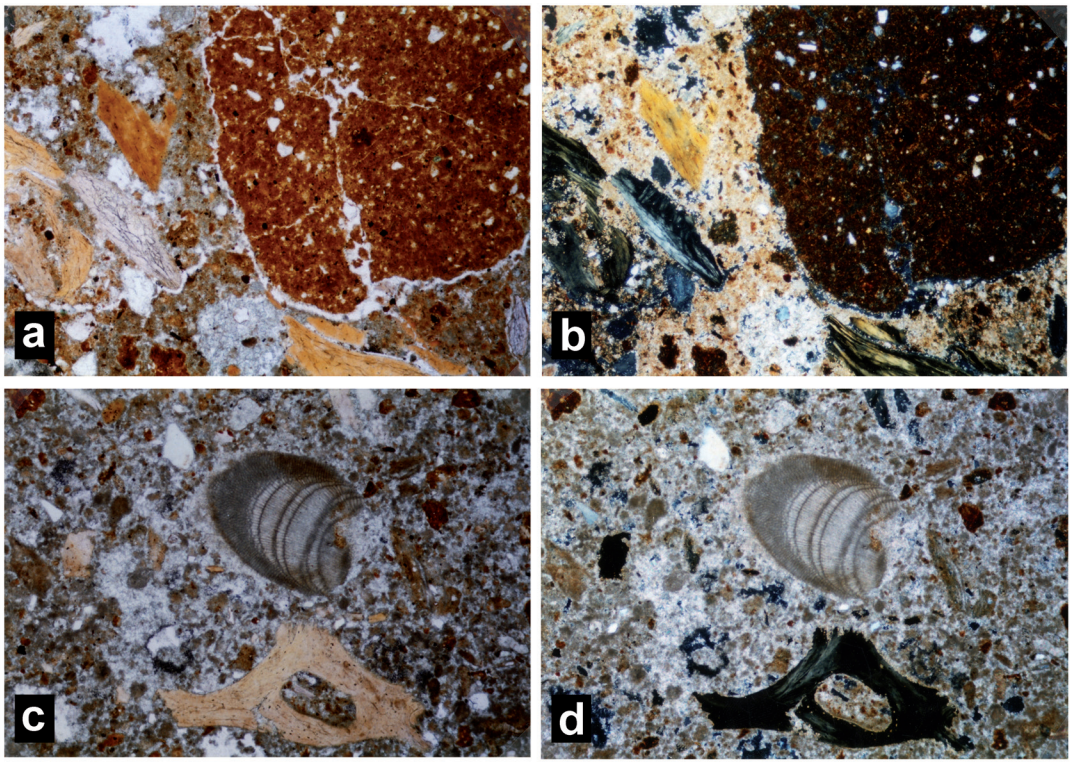

Figure 7. Microphotograph of Unit I: (a) calcite-free terra rossa aggregate (bright brown) embedded in a heterogeneous calcite-rich matrix encompassing abundant chips of bones, plane polarized light (PPL); (b) crossed polarized light, XPL; (c) well preserved shell (center) in strongly calcareous matrix, and small bone fragment (fish?) below, PPL; (d) XPL. Width of frame 2.4mm.

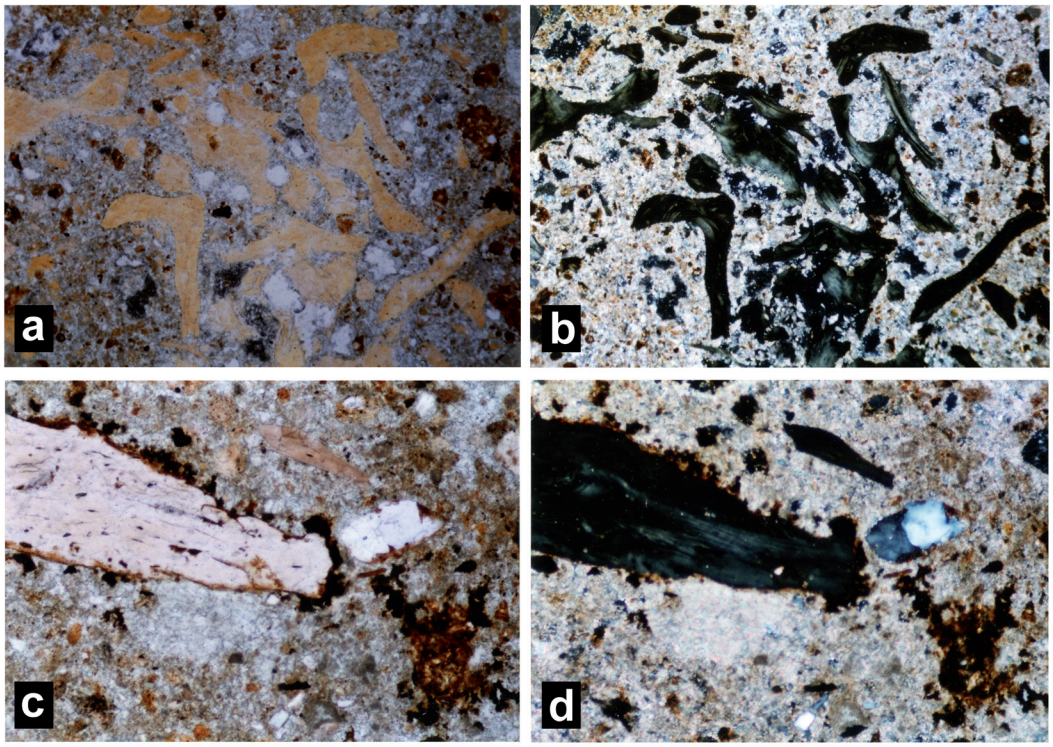

Figure 8. Microphotograph of Unit I: (a) mélange of defragmented bones, PPL; (b) XPL; Width of frame 2.4mm; (c) close up of a chip of bone with dark isotropic coating at the outer edge and small dots of the same material in the matrix (lower right), PPL; (d) XPL. Width of frame 0.97mm.

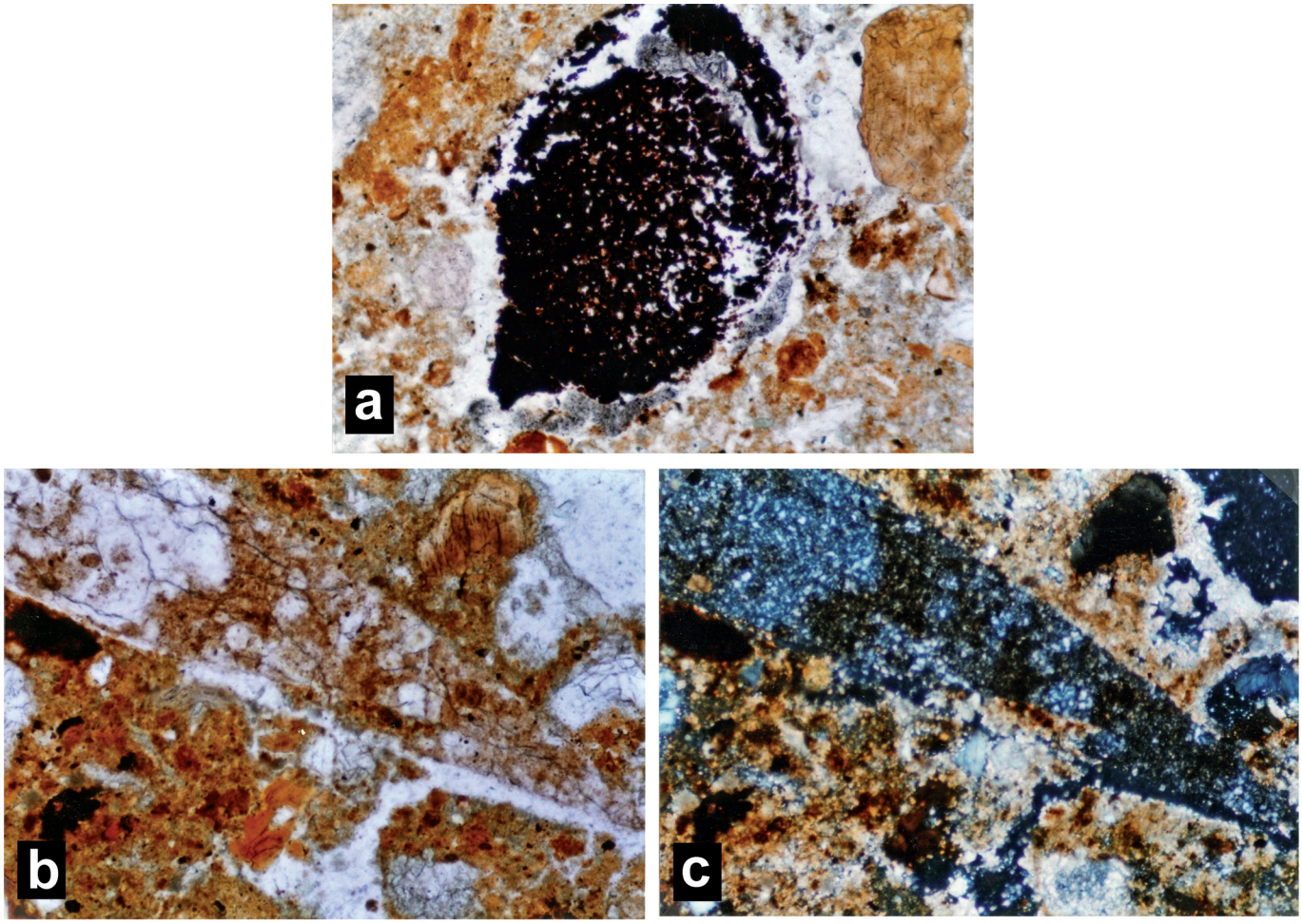

Figure 9. Microphotograph of Unit I: (a) charcoal fragment (center) of rounded shape, PPL; (b) a piece of possibly burnt flint, PPL; (c) XPL. Width of frame 2.4mm.

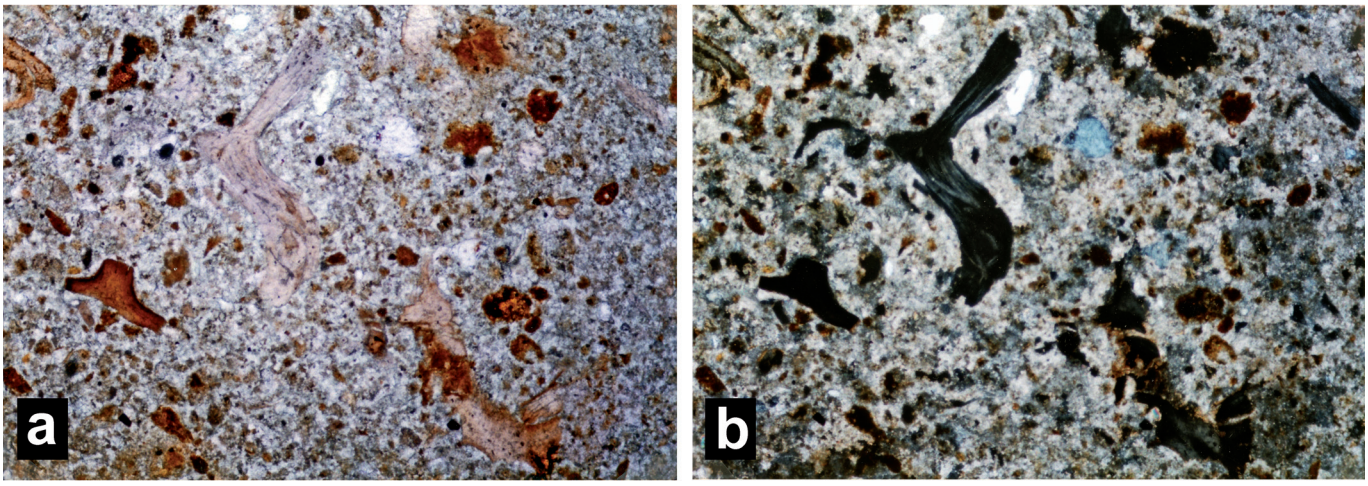

Figure 10. Unit II: Calcitic, possibly ash-derived whitish lamina incorporating small chips of bones: (a) PPL; (b) XPL. Width of frame 2.4mm.

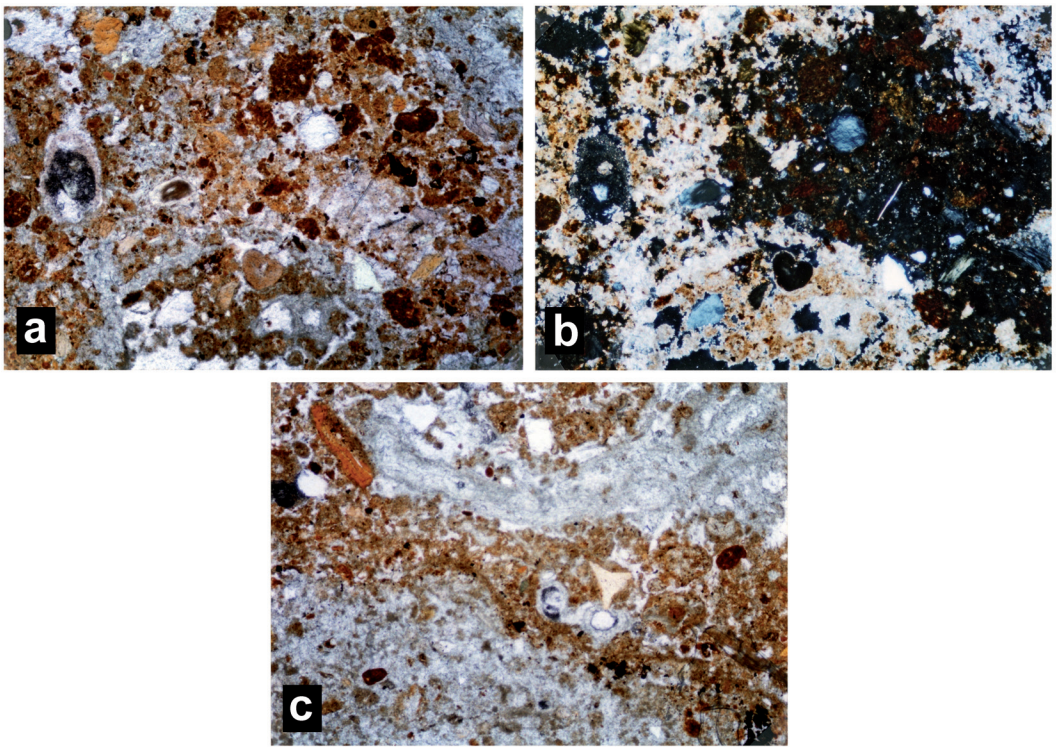

Figure 11. Unit II: Disturbed microfabric preserving two types of laminae, calcareous whitish, juxtaposed with brown isotropic: (a) PPL; (b) XPL; (c) strongly laminated patch composed of alternating whitish and brown laminae as above; note the peculiar type of fabric in the uppermost whitish lamina, testifying to travertine precipitation (PPL). Width of frame 2.4mm.

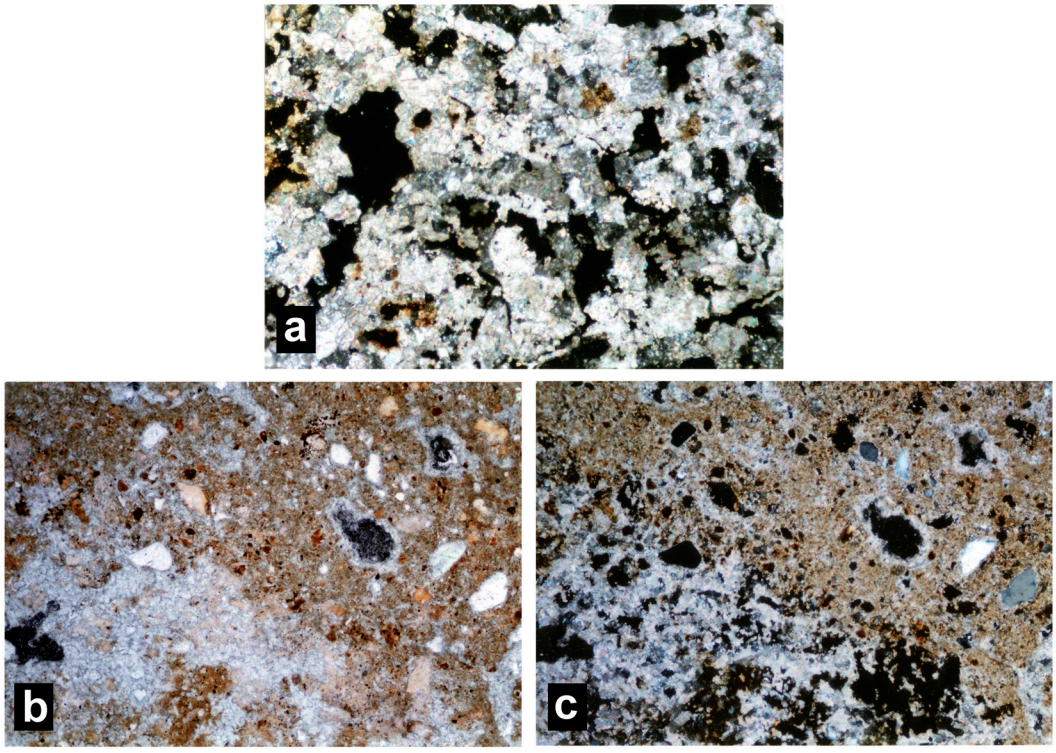

Figure 12. Unit II: (a) dolomitized limestone rock (XPL); (b) brown anthropogenic deposit superimposed on a weathered limestone stone (lower left), PPL; (c) XPL. Width of frame 2.4mm.

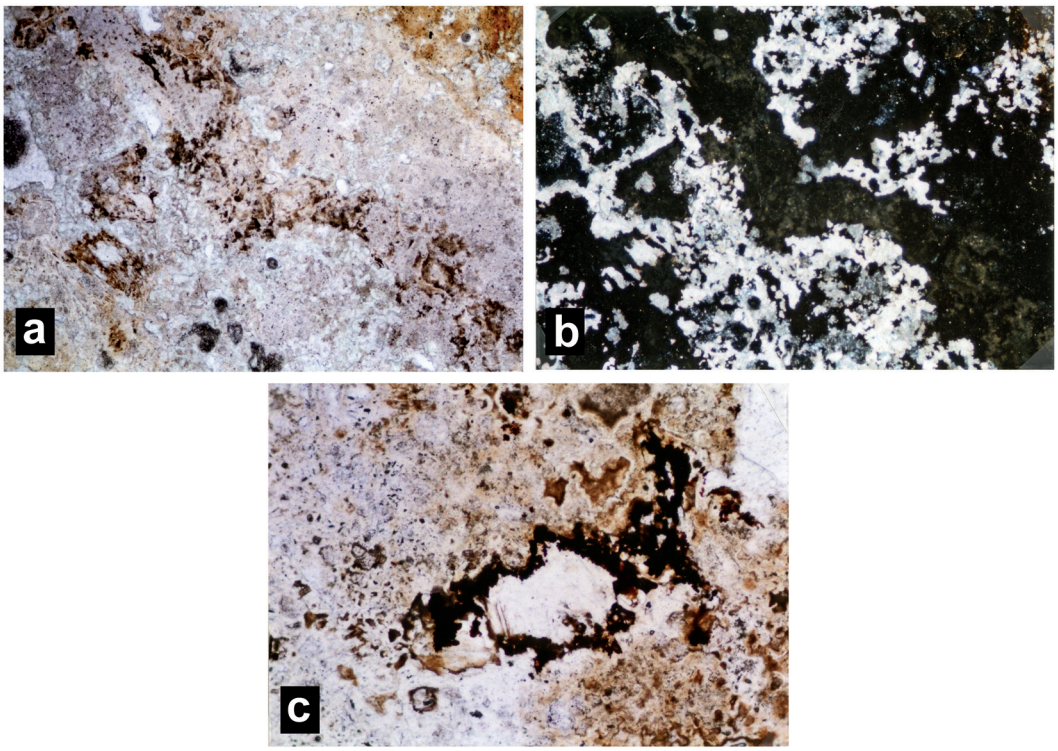

Figure 13. Weathering rinds of limestone stones in Unit II: (a) PPL; (b) XPL; Width of frame 2.4mm; (c) close up of black isotropic neofomations (PPL); Width of frame 0.97mm.

the archaeological sediments (Figure 12b and c), as well as the existence of strong weathering (Figure 13a and b), with occasional black coatings, 20–50μm in size of presumably manganese deposits (Figure 13c). Similar black coatings were also observed around certain large bones. In addition, there are aggregates of *terra rossa*, strongly defragmented in the course of either prolonged weathering, secondary calcite growth, or fire impact (Figure 14).

Unit III: Sediments of this unit include abundant charred vegetal tissues along with bones and micrite, possibly from ash-derived material. Significantly, the majority of vegetal remains appear as small elongated strips of several μm in width, occupying up to 60% of particular areas. Quantitative assessment of these areas was possible due to the large size of petrographic thin sections. For example, Figure 15a demonstrates a specific diverse microfabric clearly dominated by burnt vegetal matter. It is not always possible to identify the cellular structure of vegetal tissues because of their small size and fragmentation. Debris of cellular charred fragments are more clearly seen in Figure 15b and c. Figure 15d shows that microlaminae of these materials are completely isotropic, although they are present as a mix with fine-grained materials. In the lower part of Unit III (Figure 16) fragments of charred grasses with preserved trachea and specific walls were better preserved, although soot-like cracked fragments prevail.

Unit IV: The sediment is calcareous mixed with fine grained materials including small chips of bones, increased amount of quartz sand up to 40% in some areas (Figure 17a and b), i.e., unevenly spread within the unit, and rounded pores with thin micrite coatings. There is also evidence for secondary carbonate formation which, in contrast to the upper units, is represented by euhedral sparitic crystals, showing a quasi-radial pattern (Figure 17c and d).

SEM/EDS studies focused largely on black-colored features within thin sections. The studies were performed on a Quanta scanning electron microscope (SEM) Oxford Instruments FEA fitted with energy dispersive spectrometer (EDS) INCA 200 (Materials Engineering, Technion, Israel). The elemental composition of black-colored features in the microfabric of the sediments in L15 shows that they originated primarily from comminution of charcoal and charred vegetal remains while black stained rims of large bones and stones contain manganese (occasionally along with iron) in minor amounts only. The low amounts of manganese oxides suggest that oxidizing conditions prevailed in the studied sediments.

Mineralogical Analysis

Mineralogical study of the L15 sediments was carried out by means of Fourier Transform Infra-Red spectroscopy (FTIR) (Weiner 2010; Weiner et al. 1993, 2002). The northern section of the sounding was sampled in great detail in excavation seasons 2003–2005 and about 150 FTIR analyses were conducted. For each sample one or more representative bulk sediment samples were analyzed. In addition, many fragments that were visually different from the bulk were analyzed separately.

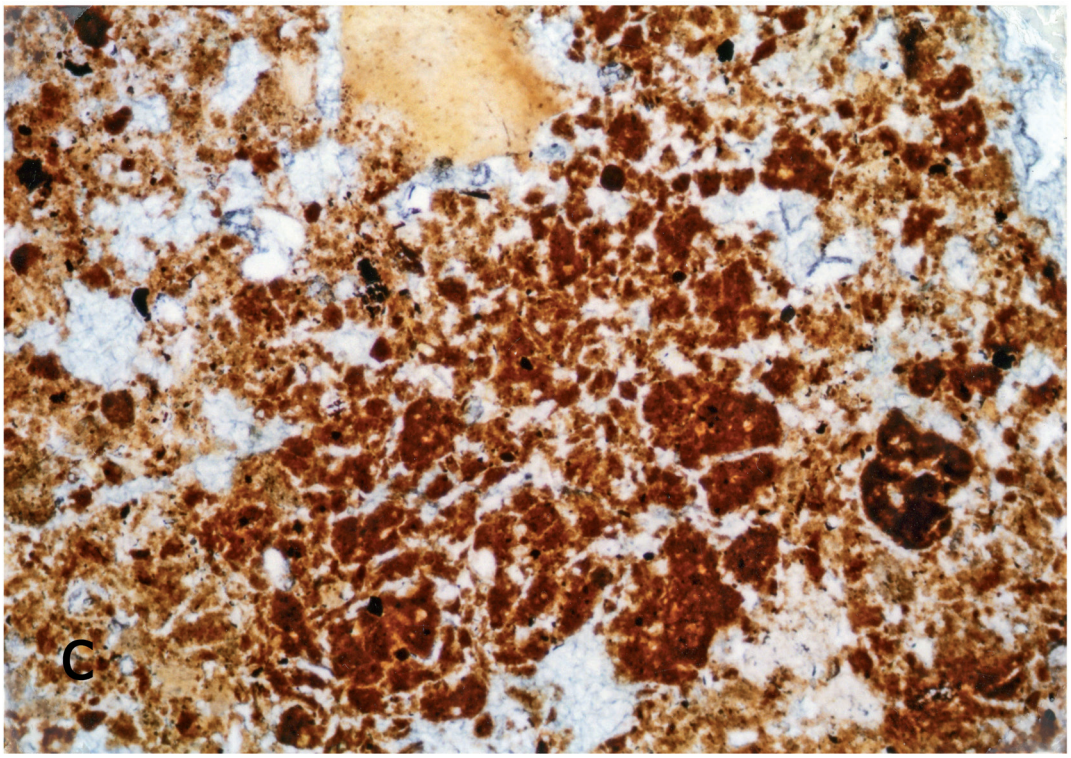

Figure 14. Unit II: Strong defragmentation (due to burning and/or trampling) of terra rossa aggregate embedded in the groundmass (PPL). Width of frame 2.4mm.

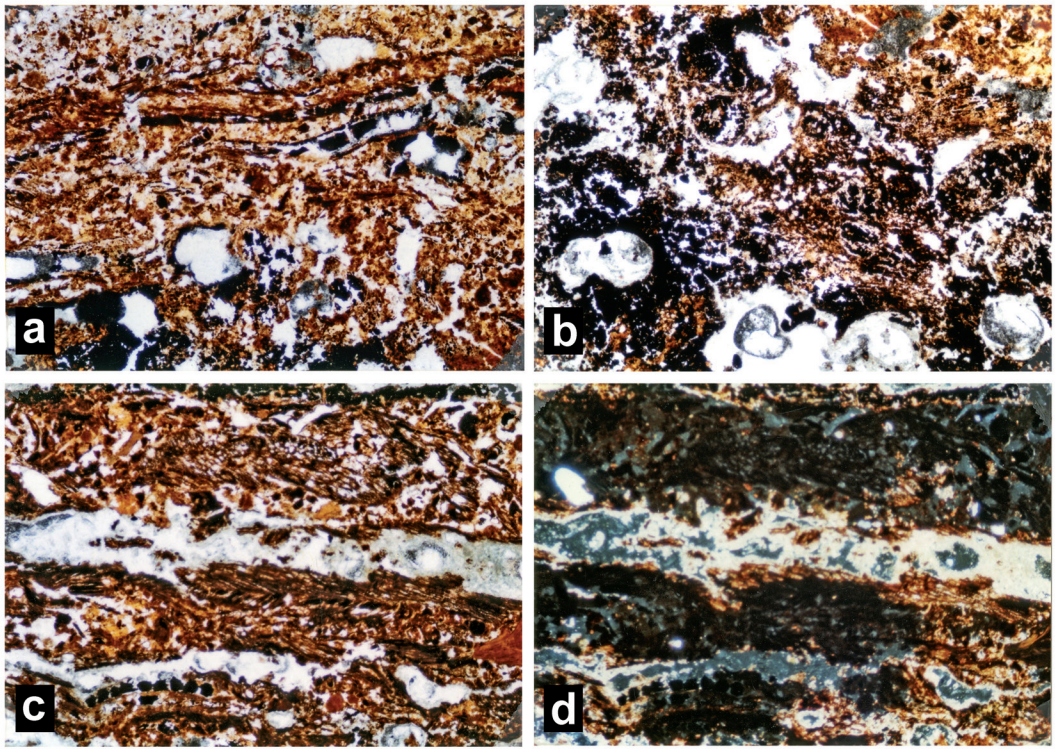

Figure 15. Horizontally placed charred tissues of grass materials in Unit III: (a) PPL; (b) another field of view (PPL); (c) another field of view; note occasional cellular structure that survived apparently low heating (PPL); (d) note the precipitation of micrite calcite in alternating laminae (XPL). Width of frame 2.4mm.

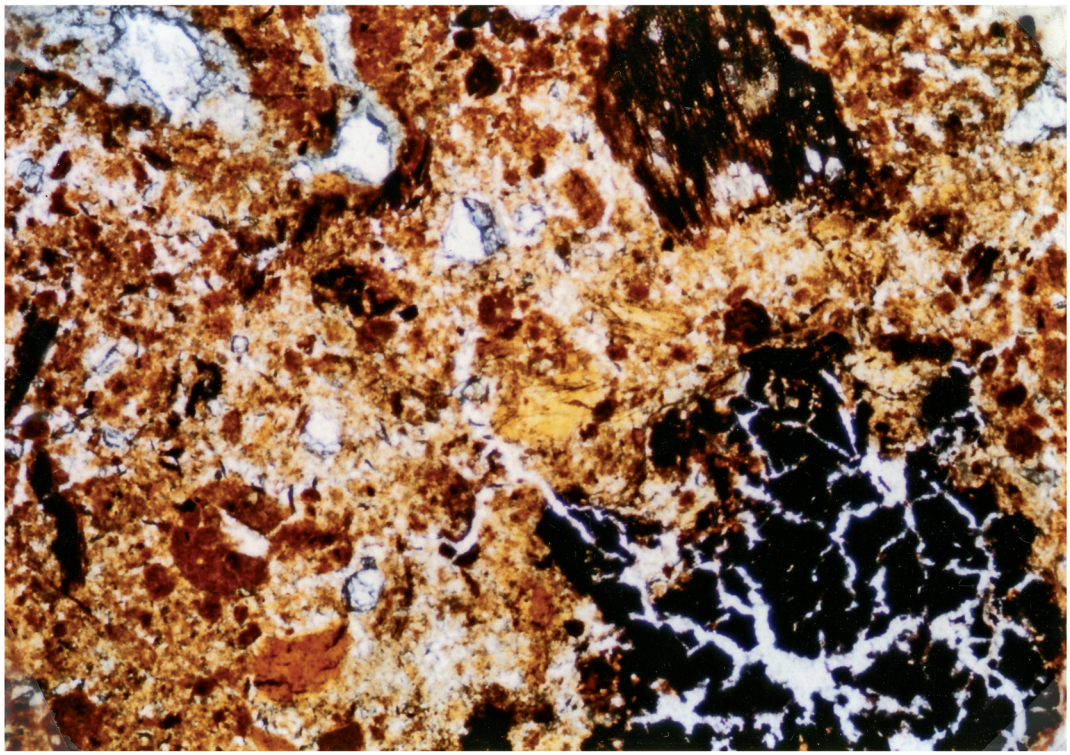

Figure 16. Two types of charred material in the lower part of Unit III: cellular-structured vegetal charred remain; the reddish-brown color suggests that it was subjected to low-temperature burning (upper right), and strongly fragmented black fragment with no cellular structure (lower right), PPL. Width of frame 2.4mm.

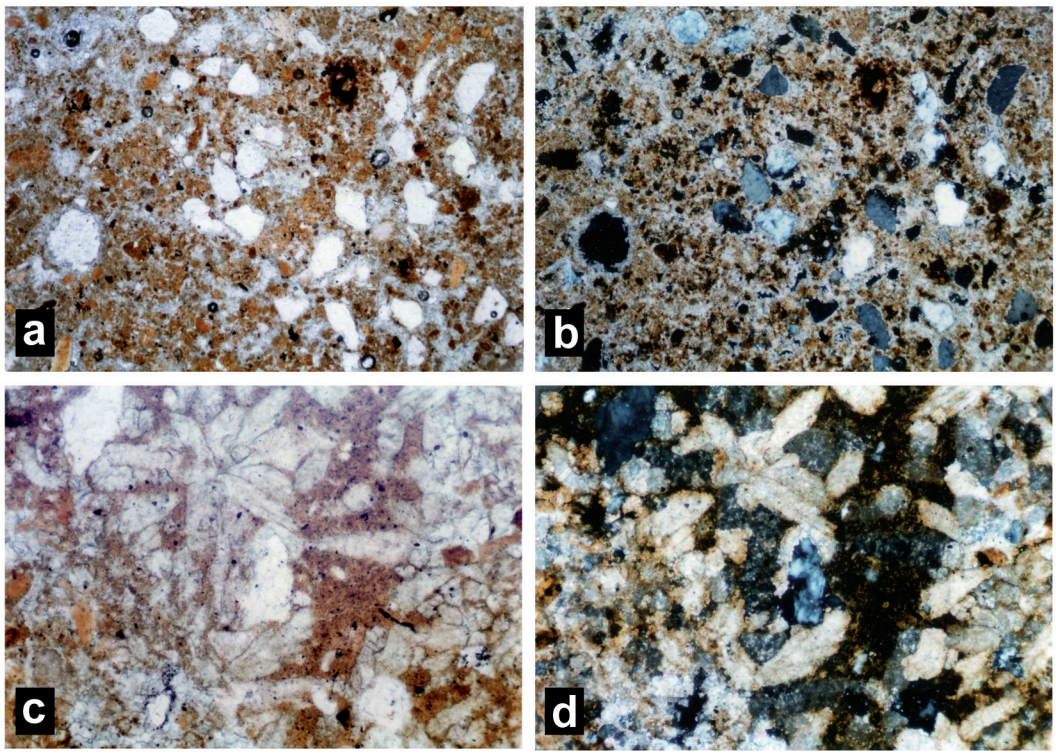

Figure 17. Anthropogenic deposit with ca. 30-40% quartz sand embedded in the clayey matrix of Unit IV: (a) PPL; (b) XPL; Width of frame 2.4mm. Precipitation of subhedral sparitic calcite (travertine), as infilling in an earlier existing pore space: (c) PPL; (d) XPL. Width of frame 0.97mm.

In almost all the bulk sediment samples, calcite is the predominant mineral phase. Based on the ratio of the two peaks at 875 and 712cm^{-1} (the ν2/ν4 ratio; Chu et al. 2008), this calcite is well crystallized. Clay is usually the second most abundant component. The clay may have undergone some structural rearrangement as the small peaks present around 3600cm^{-1} are absent in almost all samples. This can be attributed to diagenesis or to exposure to temperatures of between 400º and 600ºC (Berna et al. 2007). Almost every sample contains some carbonate hydroxylapatite (also known as dahllite) based on the presence of the peaks at 603 and 567cm^{-1}. This mineral may originate from either bones and/or authigenic precipitation. The relative amounts of carbonate hydroxylapatite vary greatly. Results are summarized following the four stratigraphic units:

Unit I: The amounts of carbonate hydroxylapatite in all these samples are very low. The bone samples analyzed vary in color and crystallinity. The yellow samples have splitting factors (as defined by Weiner and Bar-Yosef 1990) around 3.2 and the black bones have splitting factors between 3.4 and 4.3. These values indicate that the yellow bones are unburnt and are relatively well preserved, while the black bones are burnt (Stiner et al. 1995). A single white bone has a splitting factor of 5.1 and an extra hydroxyl peak at 630cm^{-1} which indicates that it was calcined at temperatures above ca. 550ºC (Stiner et al. 1995). Some samples also show the presence of charcoal.

Unit II: In general this unit contains more carbonate hydroxylapatite than Unit I. A few samples have calcite that is not well crystallized. Their ν2/ν4 ratios are around 4, indicating that they may have been originally formed as ash. At the base is a sample with relatively large amounts of clay that still maintains its original structure based on the presence of the small peaks around 3600cm^{-1}. This may indicate incorporation of *terra rossa* either during or after combustion. An additional carbonate phase, aragonite, readily identifiable by FTIR in the form of a peak at 855 cm^{-1}, was detected in specific white spots along the section. The source of aragonite is unknown but may be from shells which are originally composed of aragonite, similar to those occasionally found along the section. One such shell was identified microscopically (see Figure 7c).

Unit III: The upper ten centimeters of this unit contain large amounts of carbonate hydroxylapatite. In fact, in some samples it is the dominant component. Below this upper ten centimeters, the amounts of carbonate hydroxylapatite vary—small amounts in the middle of the section and moderately high amounts below 3.20m. This unit also contains abundant black bones and several clearly calcined ones. Opal, originating from phytoliths, has been identified in a few samples. At the base of the unit a sample containing unaltered clay was identified.

A special feature of the L15 section is the presence of stones covered by crusts or weathering rims. FTIR analysis of a crust sample indicates that its outer part is composed of hydroxylapatite, while in the inner crust calcite and clay are identifiable. The inner part of the stone is almost pure calcite.

At the base of the section, Unit IV, the presence of silicate minerals such as quartz is noticeable.

In sum, there are certain changes in mineral composition with depth along the section. The upper portion of the section is composed predominately of calcite, compared to the lower portions of the section in which clays and quartz are more pronounced. An important feature is the presence of large quantities of hydroxylapatite in the upper 10cm of Unit III. Aragonite was detected not as a component of a bulk layer but in specific speckles of whitish color. The preservation of aragonite is an indication of the good preservation of the mineral components in the cave record (Weiner 2010).

Phytolith Analysis

To date, four samples were analyzed for phytoliths, according to Albert et al. (1999) and Katz et al. (2010). A white sediment in the upper part of the sequence (sample 2003-3, Unit I) does not contain phytoliths, but has some charcoal. Gray sediment from the middle part of the sequence (sample 2004-13, Unit II) does not contain phytoliths either. Brown sediment from the lower part of the sequence (sample 2005-9, Unit IIIa) is also impoverished in phytoliths, but does contain some charcoal. Brown sediment in the lower part of the sequence (sample 2005-13, Unit IIIb) contains ca. 2 million phytoliths in 1 gr of sediment. For this sample, which is also quite rich in charcoal, there was also an indication in the FTIR spectrum for the presence of opal. The small number of identified phytoliths with consistent morphologies does not allow any quantitative determination. Qualitatively, it may be said that the morphologies identified include woody species (spherical and irregular phytoliths), some grasses (bulliform and long cell phytoliths), and phytoliths that may be attributed to either dycots or monocots (platelets).

Because most of the sediments in the studied section clearly originate from ash, the absence of phytoliths in three out of four samples is possibly due to the use of species that are devoid of phytoliths (e.g., *Salix* sp.; Tsartsidou et al. 2007). It is also possible that phytoliths dissolved due to the alkalinity of the cave water—as is evident from the precipitation of secondary calcite (see also Albert et al. 2012). We note that in Unit III an association of charred vegetal fibers and phytoliths has been identified.

THE ARCHAEOLOGICAL MATERIAL

The presented lithic and faunal assemblages constitute but a small portion of the site's rich archaeological material whose detailed lithic (Yaroshevitz et al. in press; Weinstein-Evron et al. 2003a; Weinstein-Evron and Zaidner, in preparation) and archaeozoological (Bar-Oz et al. 2004; Yeshurun et al. 2007) studies are ongoing. The specific study of the lithic and faunal remains of Square L15 was aimed at identifying changes through time and, if observed, to determine whether these correlate with the established changes in the geological and mineralogical features along the section.

TABLE 1. GENERAL BREAKDOWN OF THE LITHIC ASSEMBLAGE.

	Core	Lev. flake	Lev. point	Lev. Blade	Blade	Flake	Chunk	Burin spall	Core Trimming Elements	Tool	Total
Unit I	8	22	6	7	41	475	44	1	-	21	625
	1.3%	3.5%	1.0%	1.1%	6.6%	76.0%	7.0%	0.2%	-	3.4%	100.0%
Unit II	1	12	1	7	14	233	34	-	-	17	319
	0.3%	3.8%	0.3%	2.2%	4.4%	73.0%	10.7%	-	-	5.3%	100.0%
Unit III	20	66	2	53	93	968	58	3	13	77	1353
	1.5%	4.9%	0.1%	3.9%	6.9%	71.5%	4.3%	0.2%	1.0%	5.7%	100.0%
Unit IV	6	9	-	7	27	142	9	4	5	27	236
	1.3%	3.9%	-	3.0%	11.6%	60.9%	3.9%	1.7%	2.1%	11.6%	100.0%
Total	35	109	9	74	175	1818	145	8	18	142	2533

The Lithic Assemblage

The lithic assemblage of Square L15 includes 2,533 items larger than 2.5cm. The largest concentration derived from Unit III, but it is impossible to ascertain whether it is an indication of occupation intensity or if it rather reflects the amount of "dilution" of the archaeological material as a result of the karstic cavities from which considerable portions of the sediments were washed away, mainly in Units I and II. The massive rock at the bottom of the sequence would have had the same influence on the richness of finds within Unit IV.

The general breakdown of the assemblage by units is presented in Table 1. Flakes are the major group consisting between 61% and 76%. The frequency of laminar products is similar in Units I–III and is slightly higher in Unit IV.

Units I–III are very similar in terms of preservation of artifacts and degree of patination. Unit IV is slightly different, especially in the more developed patina and in its colors that sometimes resemble those of the Lower Paleolithic artifacts from the Lower Terrace of the site (Weinstein-Evron et al. 2003a).

Cores (Table 2) are more frequent in Square L15 than in previously studied assemblages (Weinstein-Evron et al. 2003a). Eight cores were recorded in Unit I, four of which are Levallois cores (Figure 18: 1). Three of these were knapped by the recurrent unipolar method. The desired products were blades. The fourth is a Levallois point core, worked by unipolar convergent method. One pyramidal core, a core on flake (Nahr Ibrahim; Solecki and Solecki 1970) and two small flake cores complete the core assemblage of Unit I.

In Unit II only one core was found. It was first reduced by the Levallois method but later a new debitage surface was generated on the narrow lateral side of the core and several non-Levallois blades/bladelets were removed (Figure 19).

Unit III yielded 20 cores and core fragments. Among the four Levallois cores, two are blade cores reduced by the recurrent method, one is a small preferential flake core, and

TABLE 2. CORE TYPES.

Type of Core	Unit I	Unit II	Unit III	Unit IV	Total
Levallois point core	1	-	1	-	2
Levallois blade core	3	-	2	1	6
Levallois flake core	-	-	1	-	1
Levallois core with utilization of lateral side	-	1	1	-	2
Steep surface Levallois? core	-	-	1	-	1
Core-on-flake	-	-	2	-	2
Nahr Ibrahim	1	-	5	2	8
Pyramidal core	1	-	-	-	1
Flake core	2	-	-	-	2
Broken or exploded fragments	-	-	7	3	10
Total	**8**	**1**	**20**	**6**	**35**

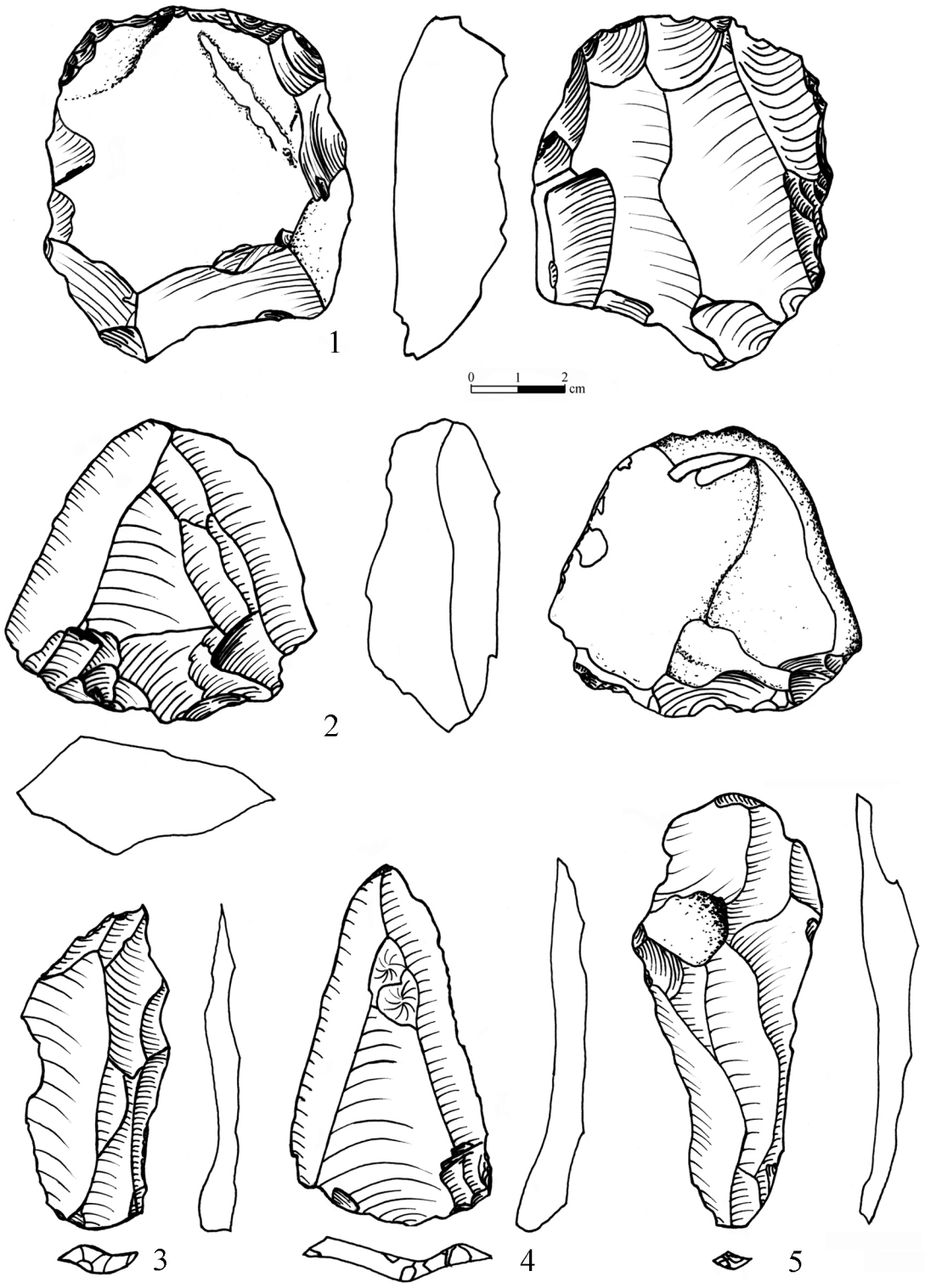

Figure 18. (1) Levallois blade core; (2) Levallois point core; (3, 5) Levallois blades; (4) Levallois point.

the fourth is a Levallois point core (Figure 18: 2).

In addition, two questionable Levallois cores were recorded. One has a flat, slightly convex Levallois-like debitage surface with a clear hierarchy between debitage and striking surfaces. Here, like in the core from Unit II, the angle of the debitage surface was changed and several blades were removed from the lateral side of the core. The second core has a flat convex debitage surface on the proximal part and a very steep convexity on the distal part. Both cores show a careful preparation of the striking platform and a convergent unipolar reduction of debitage surface which render them a triangular shape.

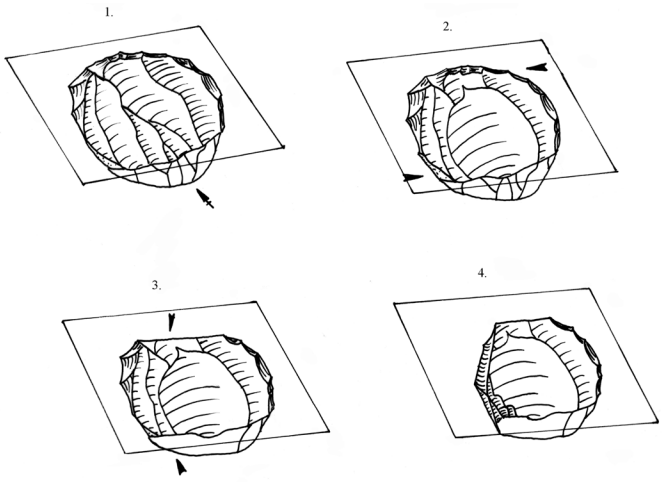

Figure 19. Schematic representation of the core from Unit II: (1) A few blades were removed from the debitage surface. (2) A large flake was removed from the same surface. (3) Striking platform was modified. (4) A few blades and bladelets were removed from the new debitage surface on the lateral narrow side of the core.

From the seven cores on flake, five are classical Nahr Ibrahim cores. Among them four were truncated on the dorsal face. They exhibit up to three removals on the ventral face. Two other cores were made on thick flakes, one with one removal and the other with three. Seven broken or fire-exploded core fragments complete the core list.

Six cores were found in Unit IV. One is a small Levallois blade core, two are Nahr Ibrahim cores, and three others are broken or fire-exploded fragments.

Significantly, no morphological or technological differences among the cores were recognized throughout the studied sequence. Levallois and Nahr Ibrahim cores appear throughout the sequence and the two Levallois(?) cores, with the utilization of the lateral side that exhibit similar ways of preparation and reduction were found in different units (Units II and III). Similarly, no variation in the state of preservation or in the intensity of exposure to fire could be observed.

The type list of the industry is presented in Table 3. For typological classification, Bordes' (1961) list was used with modifications made by Hovers (2009) and our own addition of the Hummal point (Figure 20: 4, 6). Hummal points are blades with a retouched tip that were first identified at Hummal, El Kowm oasis, Syria (Copeland 1985) and are common in the SSA of Misliya Cave (Weinstein-Evron and Zaidner in preparation; Yaroshevich et al. in press) as well.

Unretouched Levallois products are the main component of the tool assemblages of all units (Figure 18: 3–5). The number of retouched tools is generally low. It is somewhat higher in Unit IV, although caution is required because of the considerably smaller sample size. Blades were the preferred blank type chosen for retouch in all units (Table 4; Figure 20: 2–7). Even when blade frequency among the retouched pieces is lower than that of flakes, as in Units II and IV, it is still much higher than the general blade frequency in the assemblages. Unit IV is slightly different from the others not only in the higher frequency of retouched items but also in blank selection, which is more heterogeneous and less restricted to Levallois products or to blades. It also exhibits higher typological variability. In the upper three units, single side-scrapers are the dominant side-scraper group. In contrast, in Unit IV side-scrapers are a more heterogeneous group in terms of typology, selection of blanks and type of retouch. Moreover, certain side-scraper types unrecorded in the upper units appear here. A limace was also found (Figure 20: 1).

The industry of Square L15 in all four units is Levallois-Mousterian. As previously observed in the site (Weinstein-Evron et al. 2003a), the high frequency of elongated products in Units I, II, and III suggests an Early Levantine Mousterian age for the assemblages. Unit IV is more difficult to interpret. The core assemblage and the presence of Levallois items suggest a Mousterian origin. However, the variability in scraper types, including types that were not recorded in the upper units and the presence of the limace is noteworthy. While the differences can be a factor of a statistical bias due to the small size of the lithic assemblage of Unit IV, they may also indicate a true temporal development, with the occurrence of two, distinct EMP phases. The earlier, thus far represented by Unit IV, the later, commencing in the transition between Unit III and IV. The possibility that we are dealing with a pre-MP phase (most likely Acheulo-Yabrudian; Weinstein-Evron et al. 2003a) overlain by EMP habitation layers should not be ruled out.

Faunal Remains

Similar to the lithic study, the study of the faunal remains in L15 was conducted in order to identify possible temporal changes and to contribute to the understanding of the depositional and post-depositional processes represented in this section.

As mentioned above, in addition to the bones retrieved during excavation, lumps of cemented sediment, retrieved by hand-chiseling or electrical hammer digging, were subsequently treated in the laboratory, where they were chiseled carefully in an attempt to extract the embedded bone fragments. As expected, numerous bone pieces could not be extracted and many recovered bones were broken during excavation and retrieval.

For this report we collected all identifiable bone and tooth fragments, as well as all unidentifiable bone fragments (mainly shaft splinters) ≥3cm in maximum dimension. Only fragments that could be sufficiently extracted from the consolidated matrix and cleaned were chosen for analysis. All collected specimens were immersed in diluted acetic acid (10%) in order to clean the bone surfaces. The specimens were then soaked in KOH solution and rinsed with fresh water, in order to buffer the acid.

Zooarchaeological procedures followed Yeshurun et al. (2007). The specimens were identified to skeletal element and to taxon (species or size-class), using the comparative collection of the Laboratory of Archaeozoology of the Zinman Institute of Archaeology, University of Haifa. Every

TABLE 3. TYPOLOGICAL CLASSIFICATION (N=334).

	Unit I	Unit II	Unit III	Unit IV
Typical Levallois flake	29	18	119	19
Levallois point	6	-	2	-
Retouched Levallois point	-	-	2	-
Elongated Mousterian point	1	1	1	-
Limace	-	-	-	1
Single straight side-scraper	1	4	3	1
Single convex side-scraper	6	2	3	-
Single concave side-scraper	-	-	2	1
Double convex side-scraper	2	1	-	-
Convergent convex scraper	-	-	1	-
Straight transverse scraper	-	-	-	1
Side-scraper on ventral face	-	1	8	-
Abrupt-retouched side-scraper	-	-	-	1
Alternate retouch side-scraper	-	-	-	1
Typical burin	1	-	-	3
Typical borer	-	-	1	-
Naturally backed knife	-	-	12	2
Raclette	-	-	-	4
Truncated flake/blade	-	-	1	2
Notch	-	-	1	2
Denticulate	1	-	-	-
Retouch on ventral face	-	-	1	-
Miscellaneous	-	-	-	2
Retouched flake	1	5	8	-
Retouched blade	4	2	4	-
Emirah point	-	-	1	-
Use-wear	3	1	30	9
Hummal Point	1	-	1	-
Composite tool: Nahr Ibrahim with side-scraper	-	-	1	-
Total	56	35	202	49

specimen was examined under X10 magnification for bone surface modifications, induced by humans (such as butchery, burning, and fracturing), animals (rodent and carnivore gnawing) and other agents (weathering, trampling, bleaching, abrasion, and root activity) (e.g., Fisher 1995; Lyman 1994). The morphology of limb shaft fracture planes was analyzed in order to determine the stage at which the bone was broken (i.e., fresh versus dry) (Villa and Mahieu 1991).

The L15 faunal assemblage (Number of Specimens [NSP]=378) is composed mainly of compact elements such as limb bone shaft fragments (88% of studied fragments), as well as jaws and isolated teeth (6%), but a few porous elements, such as epiphyses and vertebrae fragments, also have been detected. Most of the elements are highly fragmented and virtually all limb bones retained less than half of their original circumference (Table 5). Due to the high degree of fragmentation and recovery breakage, few limb bone fracture planes could be checked. Most of them exhibited 'green' (fresh) fractures, probably as a result of opening the shafts to extract marrow.

Quantitative comparison of the concentration of faunal remains in each stratigraphic unit proved difficult, due to the non-systematic retrieval of the material and the presence of many dissolution cavities and stones throughout the section. Bone fragments were found throughout the section, with no 'sterile' layers. Nevertheless, the high number of specimens in Unit III stands out (Table 6; see also Table 5). The significant retrieval bias in the L15 assemblage can be assessed by the high frequency of modern breakage on specimens (67% of NSP) and by the under-representation of small ungulates (gazelle) compared to the previous, comprehensive study of the site's faunas (Yeshurun et al. 2007), that was conducted on samples retrieved from the

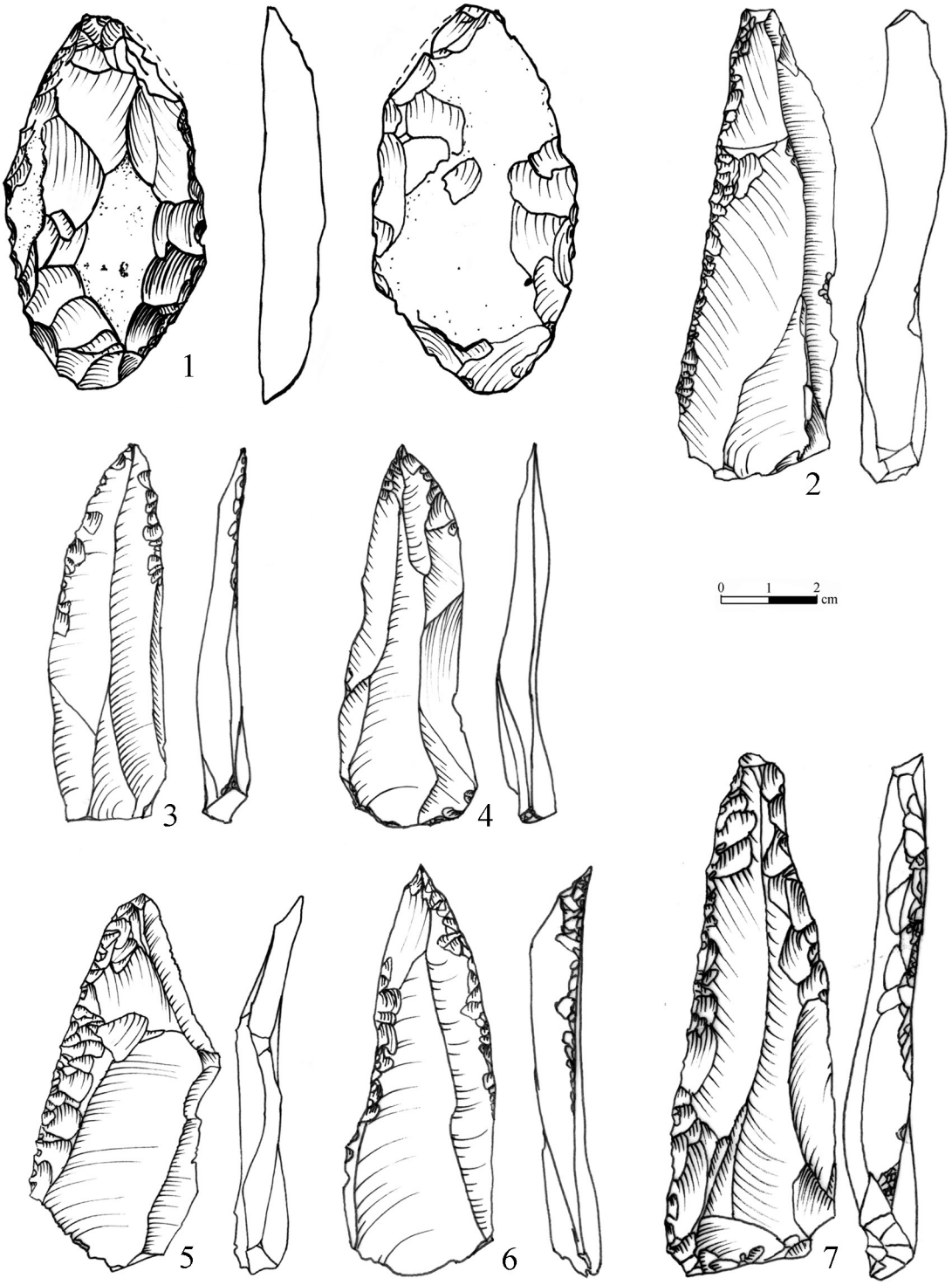

Figure 20. (1) Limace; (2, 3) Retouched blades; (4, 6) Hummal points; (5) Side-scraper; (7) Elongated Mousterian point.

softer sediments at the eastern side of the site (Squares I-N/9–10). It is likely that more gazelle elements went undetected in the cemented sediments than the larger fallow deer elements.

Bone surface modification data (see Table 5) reveals good preservation. No abraded or bleached bones were found and weathering damage is low in all units (3%). This suggests rapid burial in favorable conditions. Six

TABLE 4. BLANK SELECTION FOR RETOUCH.

	Unit I	Unit II	Unit III	Unit IV	Total
Levallois flake	4	4	7	1	16
	21.1%	25.0%	11.5%	7.1%	
Levallois point	-	-	2	-	2
	-	-	3.3%	-	
Levallois blade	-	1	8	1	10
	-	6.3%	13.1%	7.1%	
Blade	8	3	22	4	37
	42.1%	18.8%	36.1%	28.6%	
Flake	3	5	13	7	28
	15.8%	31.3%	21.3%	50.0%	
Chunk/Nodule	1	-	1	-	2
	5.3%	-	1.6%	-	
Indeterminate	3	3	8	1	15
	15.8%	18.8%	13.1%	7.1%	
Total	19	16	61	14	110
	100.0%	100.0%	100.0%	100.0%	

TABLE 5. SUMMARY OF THE TAPHONOMIC DATA OF L15, BY STRATIGRAPHIC UNIT.

UNIT		I	II	III	IV	Total
Total NSP		78	27	226	39	370
Broken by retrieval	n	56	16	153	23	248
	%	72%	59%	68%	59%	67%
Burned	n	17	11	107	11	146
	%	22%	41%	47%	28%	39%
Green fracture (angle & outline)	n	4	2	12	1	19
	of	7	2	15	1	25
	%	57%	100%	80%	100%	76%
Shaft circumference	<50	72	25	205	28	330
	>50	-	-	1	-	1
	100	-	-	-	-	-
Weathered (stage 3)	n	1	1	7	1	10
	of	75	27	213	37	352
	%	1%	4%	3%	3%	3%
Cutmarked	n	3	-	3	-	6
	%	4%	-	1%	-	2%
Gnawed (carnivore)	n	-	-	1	-	1
	%	-	-	0%	-	0%
Gnawed (rodent)	n	-	-	1	-	1
	%	-	-	0%	-	0%
Root-marked	n	43	14	82	21	160
	%	57%	52%	38%	57%	45%
Trampled	n	11	4	49	8	72
	%	15%	15%	23%	22%	20%

TABLE 6. TAXONOMIC COMPOSITION OF L15, BY STRATIGRAPHIC UNIT, ACCORDING TO THE NUMBER OF SPECIMENS[1], NUMBER OF IDENTIFIED SPECIMENS[2], AND NISP TEETH[3].

		I	II	III	IV	Total
	BASKETS	1–15	16–30	36–51	61-52	
NSP	Gg+Gg[4] size	23	16	51	10	101
	Dm+Dm[4] size	48	10	156	23	240
	Bp+Bp[4] size	7	0	19	5	35
NISP	Dm+Dm[4] size	21	4	24	8	58
	Gg+Gg[4] size	1	-	6	6	13
	Bp+Bp[4] size	1	-	4	-	6
	Sus scrofa	-	1	-	-	1
	Struthio camelus	-	-	-	1	1
	Total	23	5	34	15	79
NISP teeth	*Dama mesopotamica*	2	1	6	1	10
	Gazella gazella	0	0	2	1	3
	Bos primigenius	0	0	3	0	4
	Total	2	1	11	2	17

[1]NSP; identified as well as unidentified elements.
[2]NISP; fragments identified to body part and species/size class.
[3]Molar and premolar teeth, identified to species.
[4]Gg=*Gazella gazella*, Dm=*Dama mesopotamica*, Bp=*Bos primigenius*.

cut-marked specimens and only one carnivore-gnawed specimen were found, suggesting that the assemblage was mostly created by the human occupants of the cave. As in the soft sediments, the most notable post-depositional damage to the L15 assemblage was trampling striations (caused by either sediment compaction or human/animal agents) and root activity (see Table 5). Thirty nine percent of the specimens are burnt. When unidentified fragments are concerned, this percentage is nearly identical to the N11–12 breccia assemblage in Bar-Oz et al. (2004) and to the SSA assemblage (Yeshurun et al. 2007). The frequency of burnt, trampled, and root-marked specimens shows a marked variation between the various stratigraphic units (Figure 21). Root marks are more frequent in the higher units, while burnt bones are most abundant in Unit III.

The assemblage is taxonomically dominated by Mesopotamian fallow deer (*Dama mesopotamica*, 73% of NISP). Mountain gazelle (*Gazella gazella*, 16%) and aurochs (*Bos primigenius*, 8%) are also present. A wild boar (*Sus scrofa*) phalanx and an ostrich (*Struthio camelus*) egg-shell fragment were also found (see Table 6). No remains of smaller mammals, birds, reptiles, and fish were found. This taxonomic composition is more or less consistent throughout the section (see Table 6, Figure 22), with the exception of Unit II, perhaps due to the small sample size of this unit.

In sum, the faunal assemblage retrieved from the L15 section represents carcass parts acquired, consumed, and discarded by humans. Other pre- or post-depositional agents did not play an important role in the assemblage formation. This conclusion, coupled with the taxonomic diversity, makes the L15 assemblage similar to the other Upper Terrace assemblages (Bar-Oz et al. 2004; Yeshurun et al. 2007), perhaps representing similar habitations and conditions of accumulation.

DISCUSSION

Misliya is a collapsed cave whose remains are scattered over and within the archaeological layers, mainly in the form of large bedrock boulders and flowstones. Several

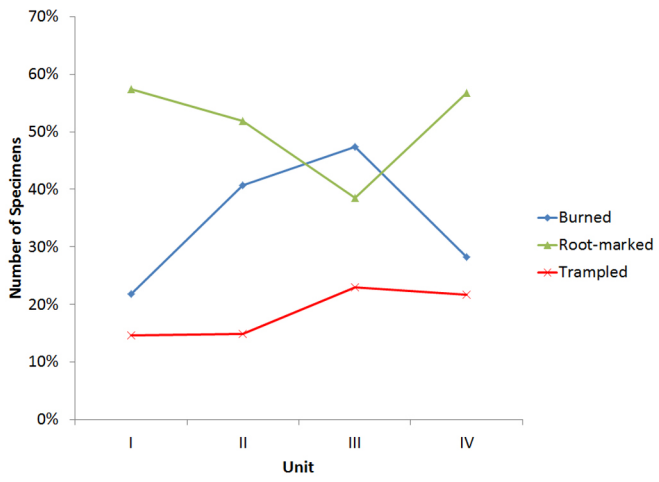

Figure 21. Frequencies of trampled, burned and root-marked specimens in each geological unit. Data are from Table 5.

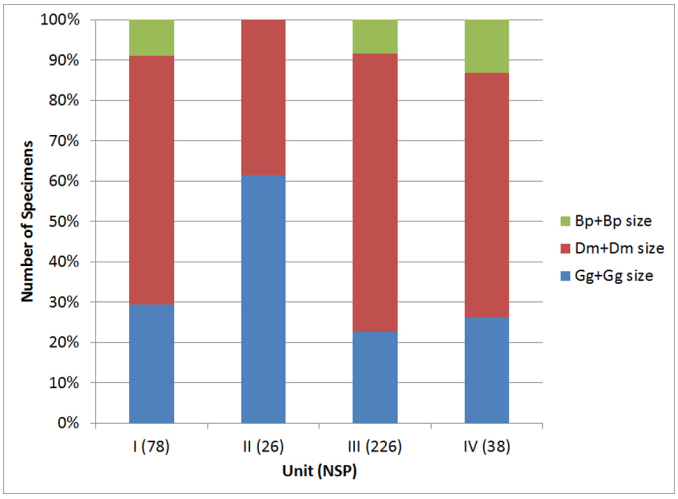

Figure 22. Relative abundance of size-classes in each geological unit. NSP values are given for each column. Data are from Table 6.

boulders had rolled some distance down the slope. The area covered by the archaeological sediments roughly delineates the extent of the paleo-cave which extended ~30m westward from the present cliff face during the Acheulo-Yabrudian and has gradually retreated eastward ever since.

The present research deals with the EMP habitation of the cave, as indicated by both the available dates and the techno-typological characteristics of the lithic industry, that are roughly similar to other Levantine EMP occurrences (e.g., at Tabun and Hayonim caves; Garrod and Bate 1937; Jelinek 1982; Meignen 1998). The study deals with a spatially limited area that was, however, dug to considerable depth. Thus, the results concern mainly temporal developments and suggest a long period of repeated habitations of a seemingly single cultural tradition. The lithics are typical of the EMP throughout, with the doubtful exception of the very bottom of the sequence. The faunal remains, which are the result of human subsistence behavior, likewise do not reveal any significant temporal change.

While temporal changes are mainly registered in our deep sounding, spatial factors are also at play here. Indeed, it is the relative location of the studied section in relation to the cave's walls and ceiling that had been 'spatially' changed and the variations in the sediments of the studied 'window' can thus provide important insights into changes in the cave's configuration through time. Together with field observations, laboratory analyses help reconstruct some crucial moments in the geological history of the cave during its occupation by EMP humans. The Misliya Cave sequence can be roughly divided into two main parts, the lower encompassing Units III and IV and the upper one, consisting of Units I and II. Between the lower and upper part, there is an apparent disconformity. The following discussion is presented from bottom to the top, thus allowing a time-ascending reconstruction of various processes and events (Figure 23).

The cultural affinity and the nature of Unit IV are not fully comprehended yet, due to its very limited exposure. A massive rockfall of huge boulders (or bedrock), one of which was encountered at the bottom of Square L15, underlies the EMP sequence. The lowermost deposit is rather clay rich, albeit with admixture of quartz sand and silt which may have been wind-blown from the adjacent coastal plain. However, fine materials may have also derived from *terra rossa* soils, slumped into the cave as is known in other Levantine sites, e.g., Tabun (Albert et al. 1999; Tsatskin 2000). Significantly, only two samples of clay analyzed by FTIR (close to the bases of Unit III and Unit II) showed small peaks around 3600cm^{-1} of OH groups incorporated in the original structure of phyllosilicates. This is indicative of unheated clay.

Unit III exhibits the best preserved macro- and microstructures, in particular, excellently preserved humified and/or charred plant material arranged in micro-laminae. The good preservation of these features indicating *in situ* human activities resulted apparently from rapid burial of the sediments. This organic matter is contained in the context of well-preserved hearths, which also contain both blackened and calcined burnt bones. It is therefore suggested that human activities in this part of the cave during Unit III formation were related to fire use. The association of materials affected by various temperature regimes, e.g., high temperature calcined bones along with low temperature organic matter humification, suggests variability in function and location of hearths.

Many prehistoric cave deposits in the southern Levant show prominent sedimentological features associated with the human use of fire (Goldberg and Bar Yosef 2005). For example, anthropogenic deposits are revealed as a series of well-delineated hearths with alternating black, white, and reddish coloration in Kebara Cave (Meignen et al. 2007) and Hayonim Cave (Bar-Yosef et al. 2005), which is chronologically closer to Misliya. The hearths were shown to contain both wood charcoal and charred grass (Woodward and Goldberg 2001), and a fraction of siliceous materials derived from wood ash (Schiegl et al. 1996), as well as burnt bones in different degrees of preservation and stages of thermal impact (Weiner et al. 2002).

At Misliya, in addition to black lenses of mainly charred grass tissues, there are reddish lenses probably derived from burnt clayey *terra rossa* and hard gray lenses that are composed of micritic calcite. Pseudomorphs of calcite after calcium oxalate crystals were observed in thin sections. It is therefore concluded that the cemented calcite lenses here originated from partial dissolution and re-precipitation of calcitic wood ash. This phenomenon was noted in Amud and Qesem caves (Karkanas et al. 2007; Shahack-Gross et al. 2008). Wood ash is composed of microcrystalline calcite. This attribute indicates that the surface to bulk ratio is very high, which makes these crystallites highly soluble. In alkaline conditions wood ash will dissolve only partially and upon drying authigenic micritic and sparitic calcite will form (Courty et al. 1989; Shahack-Gross and Ayalon in press). Under such conditions cemented ash will be composed of all the components observed in this study—micritic and sparitic calcite, a few preserved ash pseudo-

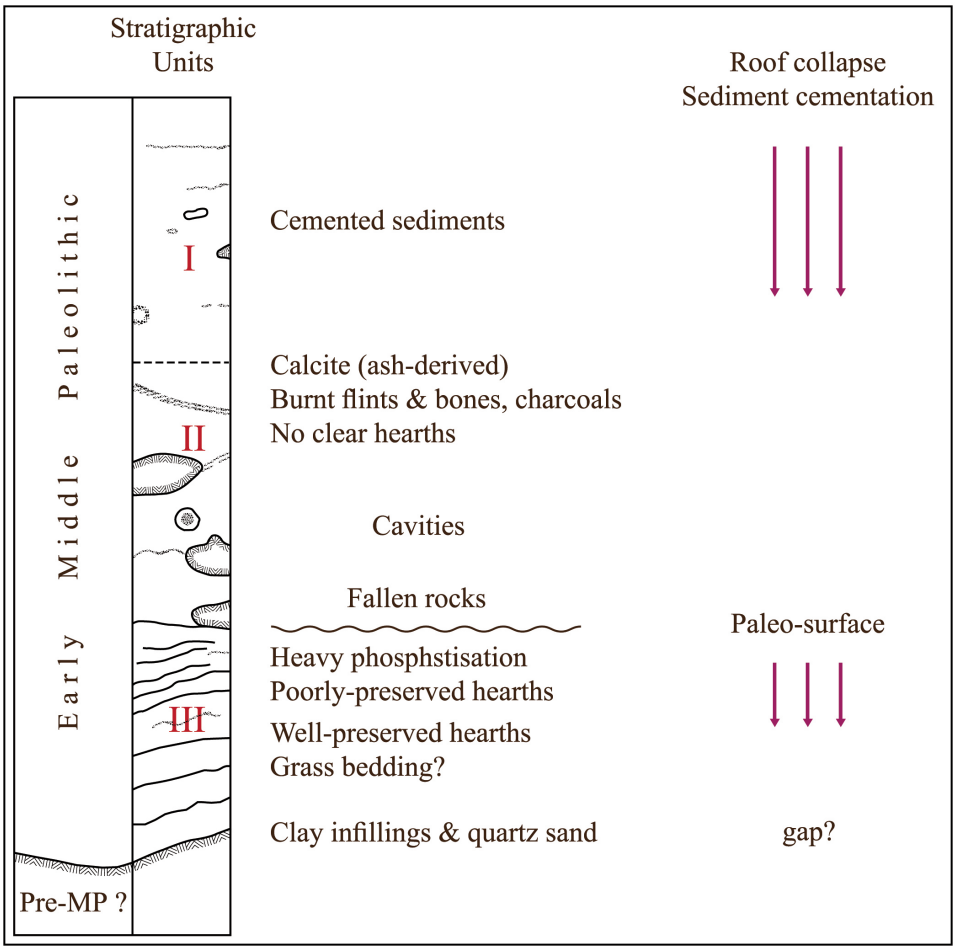

Figure 23. Reconstruction the cave's geological history based on the deep L15 sounding.

morphs, charred vegetal matter, carbonized and calcined bones, and occasional heated clay aggregates.

The exceptional preservation of vegetal tissues at Misliya is noteworthy. At Misliya, these (partially) charred remains are spatially identified in a central part of the collapsed cave, associated with wood ash, burnt bones, and phytoliths. Similar attributes have been recently reported from later MP and MSA sites in Spain (Esquilleu Cave; Cabanas et al. 2010) and South Africa (Sibudu rockshelter; Goldberg et al. 2009; Wadley et al. 2011). At Esquilleu Cave, bedded phytoliths have been identified in the central part of the site, associated with remains of wood ash, burnt clay, and charred vegetal matter (Cabanes et al. 2010; Mallol et al. 2010). At Sibudu rockshelter, the bedded phytoliths have been identified along the shelter's wall, associated with wood ash, charred vegetal fibers, and burnt bones (Goldberg et al. 2009). We note that at the macroscopic scale it was impossible to identify these microlaminations, possibly due to the cementation processes. Yet, based on the micromorphological similarity of the bedded vegetal remains and associated materials in Misliya to those at Esquilleu and Sibudu, we offer the preliminary suggestion that these tissues represent the remains of bedding or matting.

The upper part of Unit III (sub-unit IIIa) is generally similar to its lower part, but is poorly preserved and its features disrupted. The top 10cm of this sub-unit are extremely rich in authigenic carbonated hydroxylapatite.

The upper Units I–II seem to lie unconformably upon Unit III, indicating a gap in deposition and/or erosion at this phase. No phosphate minerals other than carbonate hydroxylapatite are found here, indicating that the pH always remained above 7 (Weiner 2010). As the source of the phosphate is most likely from bat guano (Jelinek et al. 1973; Shahack-Gross et al. 2004), the extent of phosphatization can be an indication of the existence of a roof above Square L15. The fact that the upper ten centimeters of Unit III are heavily phosphatized, is consistent with this having been a paleo-surface. We suggest that the high concentration of carbonated hydroxylapatite indicates a period of abandonment (at least of this part of the cave) in which bats could have inhabited the cave, thus depositing large amounts of guano that released phosphate into the top part of Unit IIIa. This, in turn indicates that the area was still not only covered by a roof, but also may have been enclosed by the cave walls and probably far enough from its entrance to enable bat habitation. The occurrence of unmodified clay at the base of Unit II may also indicate that the cave was not inhabited during this time. The disruption of bedding

laminae at the top of Unit III may have resulted from strong diagenesis possibly due to phosphatization.

The upper part of the sequence, Units I–II, is different from its lower portions in its general massive structure, erosional cavities, large quantities of fallen stones, and the absence of discrete hearths and bedding features. Even though no distinct burnt-material lenses were observed, there is ample evidence for fire-inflicted modification on the sediments and their archaeological content. For example, the high ratio of burnt bones (see Table 5) in Unit II (41%) is close to that of Unit III (47%) where hearths were clearly identified. It is not clear whether hearths were not constructed here at this habitation phase or if constructed, they were subjected to more severe diagenesis and were thus more poorly preserved than those of the earlier cycle. Abundant evidence of post-depositional processes exists at the lower part of this phase in the form of phosphate weathering rims around the stones. Given that the entire circumference of the stone is covered with a phosphatic rim, the process of geochemical transformation was plausibly triggered by the impact of P-bearing water solutions seeping through the sediments. If so, this occurred when the deposits were more or less sheltered by the roof. The fair amount of carbonate hydroxylapatite in bulk sediments supports our suggestion. The abundant fallen rocks may indicate that the process of roof degradation and collapse at this part of the cave had already started. It culminated during the time of deposition of Unit I.

CONCLUSIONS

The EMP sequence at Misliya Cave was deposited under the cave roof whose westward extension retreated gradually. We distinguished two main sedimentological cycles and possibly also occupational phases above a massive rockfall (or bedrock), separated by a gap of undetermined duration that was, however, long enough to create a distinct paleosurface.

Anthropogenic features are best preserved in the lower part of the sequence. The evidence for charred bedding at Misliya constitutes the earliest finding of such a feature to date. Unit III was deposited before the roof of the cave collapsed and the cave was rather closed. In contrast, Unit II sediments accumulated when the roof of the cave started to collapse and the cave was apparently more open. The gradual collapse of the cave continued during the sedimentation of Unit I.

It was only after the roof had fully collapsed (and was certainly closer to its present location, 4m east of the L15 section) that the upper deposits (Unit I) were cemented, as a result of rain water and exposure to the elements. The gradual spatial softening of the cemented sediments eastward supports the notion of a gradually receding roof.

It is unclear when exactly the cave attained its present form. However, because the extent of the cemented layers closely conforms to the present-day drip-line, the last major collapse was most probably the one that exposed the studied Square L15 to the elements.

ACKNOWLEDGEMENTS

In memory of Dan David, a dear friend and an enthusiastic supporter of the Misliya Cave project. D. Friesm and I. Hananni prepared the infrared spectra. Figures were produced by Anat Regev-Gisis. Thanks are due to Daniel Kaufman, Simcha Lev-Yadun, and Ron Shimelmitz for their remarks. The Misliya excavations are supported by the Dan David Foundation, the Leakey Foundation, the Irene Levi-Sala Care Arcaheological Foundation, and the Faculty of Humanities, the University of Haifa (by whom it is coined the "Faculty Cave").

REFERENCES

Albert, R.M., Lavi, O., Estroff, L., Weiner, S. Tsatskin, A., Ronen, A., and Lev-Yadun, S. 1999. Mode of occupation of Tabun Cave, Mount Carmel, Israel during the Later Mousterian: a study of sediments and phytoliths. *Journal of Archaeological Science* 26, 1249–1260.

Albert, R.M., Berna, F., and Goldberg, P. 2012. Insights on Neanderthal fire use at Kebara Cave (Israel) through high resolution study of prehistoric combustion features: evidence from phytoliths and thin sections. *Quaternary International* 247, 278–293.

Bar-Oz, G., Weinstein-Evron, M., Livne, P., and Zaidner, Y. 2004. Fragments of information: preliminary taphonomic results from the Middle Palaeolithic breccia layers of Misliya Cave, Mount Carmel, Israel. In: *Biosphere to Lithosphere: New Studies in Vertebrate Taphonomy*, O'Connor, T. (ed.). Oxbow Press, Oxford, pp. 128–136.

Bar-Yosef, O. 1998. The chronology of the Middle Paleolithic of the Levant. In: *Neandertals and Modern Humans in Western Asia*, Akazawa, T., Aoki, K., and Bar-Yosef, O. (eds.). Plenum Press, New York, pp. 39–56.

Bar-Yosef, O., Belfer-Cohen, A., Goldberg, P., Kuhn, S.L., Meignen, L., Vandermeerch, B., and Weiner, S. 2005. Archaeological background to Hayonim Cave and Meged Rockshelter. In: *The Faunas of Hayonim Cave, Israel: A 200,000-year Record of Paleolithic Diet, Demography and Society*, Stiner, M.C. American School of Prehistoric Research, Peabody Museum, Cambridge, Massachusetts, Bulletin 48, pp. 17–38.

Berna, F., Behar, A., Shahack-Gross, R., Berg, J., Boaretto, E., Gilboa, A., Sharon, I., Shalev, S., Shilshtein, S., Yahalom-Mack, N., Zorn, J.R., and Weiner, S. 2007. Sediments exposed to high temperatures: reconstructing pyrotechnological processes in Late Bronze and Iron Age Strata at Tel Dor (Israel). *Journal of Archaeological Science* 34, 358–373.

Bordes, F. 1961. *Typologie du Paleolithique Ancien et Moyen*. Éditions du CNRS, Paris.

Bullock, P., Federoff, N., Jongerius, A., Stoops, G., and Tursina, T. 1985. *Handbook for Soil Thin Section Description.* Waine Research Publications, Wolverhampton.

Cabanes, D., Mallol, C., Exposito, I., and Baena, J. 2010. Phytolith evidence for hearths and beds in the late Mousterian occupations of Esquilleu cave (Cantabria, Spain). J*ournal of Archaeological Science* 37, 2947–2957.

Chu, V., Regev, L., Weiner, S., and Boaretto, E. 2008. Differentiating between anthropogenic calcite in plaster, ash and natural calcite using infrared spectroscopy: implications in archaeology. *Journal of Archaeological Science* 35, 905–911.

Copeland, L. 1975. The Middle and Upper Palaeolithic in Lebanon and Syria in the light of recent research. In: *Problems in Prehistory: North Africa and the Levant*, Wendorf, F., Close, A. (eds.). Southern Methodist University Press, Dallas, pp. 317–350.

Copeland, L. 1985. The pointed tools of Hummal Ia (El Kowm, Syria). *Cahiers de l'Euphrate* 4. Éditions Rechrche sur les Civilisations, Paris, pp. 177–189.

Courty, M.-A., Goldberg, P., and Macphail, R. 1989. *Soils and Micromorphology in Archaeology*. Cambridge University Press, New York.

Fisher, J.W. 1995. Bone surface modifications in zooarchaeology. *Journal of Archaeological Method and Theory* 2, 7–68.

Garrod, D.A.E. and Bate, D.M.A. 1937. *The Stone Age of Mount Carmel. Vol. I. Excavations at the Wady el-Mughara*. Clarendon Press, Oxford.

Goldberg, P. and Bar-Yosef, O. 2005. Cave dwellers in the Middle East. In: *Encyclopedia of Caves*, Culver, D. and White, W. (eds.). Elsevier Academic Press, San Diego, pp. 85–89.

Goldberg, P., Miller, C.E., Schiegl, S., Ligouis, B., Berna, F., Conard, N.J., and Wadley, L. 2009. Bedding, hearths, and site maintenance in the Middle Stone Age of Sibudu Cave, KwaZulu-Natal, South Africa. *Archaeological and Anthropological Sciences* 1, 95–122.

Grün, R. and Stringer, C. 2000. Tabun revisited: revised ESR chronology and new ESR and U-series analyses of dental material from Tabun CI. *Journal of Human Evolution* 39, 601–612.

Hovers, E. 2009. *The Lithic Assemblages of Qafzeh Cave*. Oxford University Press, New York.

Jelinek, A.J. 1982. The Middle Palaeolithic in the Southern Levant, with comments on the appearance of modern *Homo sapiens*. In: *The Transition from Lower to Middle Palaeolithic and the Origin of Modern Man*, Ronen, A. (ed.). BAR International Series, Oxford, pp. 57–104.

Jelinek, A.J., Farrand, W.R., Hass, G., Horowitz, A., and Goldberg, P. 1973. New excavations at the Tabun Cave, Mount Carmel, Israel: a preliminary report. *Paléorient* 1(2), 151–183.

Karkanas, P., Shahack-Gross, R., Ayalon, A., Bar-Matthews, M., Barkai, R., Frumkin, A., Gopher, A., and Stiner, M. 2007. Evidence for habitual use of fire at the end of the Lower Paleolithic: site formation processes at Qesem Cave, Israel. *Journal of Human Evolution* 53, 197–212.

Katz, O., Cabanes, D., Weiner, S., Maeir, A.M., Boaretto, E., and Shahack-Gross, R. 2010. Rapid phytolith extraction for analysis of phytolith concentrations and assemblages during an excavation: an application at Tell es-Safi/Gath, Israel. *Journal of Archaeological Science* 37, 1557–1563.

Karcz, Y. 1958. *The Geology of the Northeastern Carmel*. MSc Thesis, The Hebrew University of Jerusalem.

Lyman, R.L. 1994. *Vertebrate Taphonomy*. Cambridge University Press, Cambridge.

Mallol, C., Cabanes, D., and Baena, J. 2010. Microstratigraphy and diagenesis at the Upper Pleistocene site of Esquilleu Cave (Cantabria, Spain). *Quaternary International* 214, 70–81.

Meignen, L. 1998. Hayonim Cave lithic assemblage in the context of the Near Eastern Middle Paleolithic. In: *Neandertals and Modern Humans in Western Asia*, Akazawa, T., Aoki, K., and Bar-Yosef, O. (eds.). Plenum Press, New York, pp. 165–180.

Meignen, L. 2011. The contribution of Hayonim cave assemblages to the understanding of the so-called Early Levantine Mousterian. In: *The Lower and Middle Paleolithic in the Middle East and Neighboring Regions*, Le Tensorer, J.-M., Jagher, R., and Otte, M. (eds.). ERAUL 126, pp. 85–100.

Meignen, L. and Bar-Yosef, O. 1992. Middle Paleolithic variability in Kebara Cave, Israel. In: *The Evolution and Dispersal of Modern Humans in Asia*, Akazawa, T., Aoki, K., and Kimura, T. (eds.). Hakusen-Sha, Tokyo, pp. 129–148.

Meignen, L., Bar-Yosef, O., Speth, J.D., and Stiner, M.C. 2006. Middle Paleolithic settlement patterns in the Levant. In: *Transitions Before the Transition: Evolution and Stability in the Middle Paleolithic and Middle Stone Age*, Hovers, E. and Kuhn, S.L. (eds.). Springer, New York, pp. 149–169.

Meignen, L., Goldberg P., and Bar-Yosef O. 2007. The hearths at Kebara Cave and their role in site formation processes. In: *Kebara Cave, Mt. Carmel, Israel: The Middle and Upper Paleolithic Archaeology, Part I*, Bar-Yosef, O., Meignen, L. (eds.). American School of Prehistoric Research, Peabody Museum, Cambridge, Massachusetts, Bulletin 49, pp. 91–122.

McCown, T.D. 1937. Mugharet es-Skhul: description and excavations. In: *The Stone Age of Mount Carmel: Excavations at the Wady el-Mughara*, Vol. I., Garrod, D.A.E. and Bate, D.M.A. Clarendon Press, Oxford, pp. 91–112.

Mercier, N. and Valladas, H. 2003. Reassessment of TL age estimates of burnt flints from the Palaeolithic site of Tabun Cave, Israel. *Journal of Human Evolution* 45, 401–409.

Mercier, N., Valladas, H., Frojet, L., Joron, J.-L., Ryess, J.-L., Weiner, S., Goldberg, P., Meignen, L., Bar-Yosef, O., Belfer-Cohen, A., Chech, M., Kuhn, S.L., Stiner, M.C., Tillier, A.-M., Arensburg, B., and Vandermeersch, B. 2007. Hayonim Cave: a TL-based chronology for this Levantine Mousterian sequence. *Journal of Archaeological Science* 34, 1064–1077.

Rink, W.J., Richter, D., Schwarcz, H.P., Monigal, K., and Kaufman, D. 2003. Age of the Middle Palaeolithic site of Rosh Ein Mor, Central Negev, Israel: implications for the age range of the Early Levantine Mousterian of the Levantine Corridor. *Journal of Archaeological Science* 30, 195–204.

Rink, W. J., Schwarcz, H. P., Lee, H. K., Rees-Jones, J.,

Rabinovich, R., and Hovers, E. 2001. Electron Spin Resonance (ESR) and Thermal Ionization Mass Spectrometric (TIMS) $^{230}Th/^{234}U$ dating of teeth in Middle Palaeolithic layers at Amud Cave, Israel. *Geoarchaeology* 16(6), 701–717.

Rink, W. J., Schwarcz, H. P., Weiner, S., Goldberg, P., Meignen, L., and Bar-Yosef, O. 2004. Age of the Mousterian industry at Hayonim Cave, Northern Israel, using Electron Spin Resonance and $^{230}Th/^{234}U$ Methods. *Journal of Archaeological Science* 31, 953–964.

Schiegl, S., Goldberg, P., Bar-Yosef, O., and Weiner S. 1996. Ash deposits in Hayonim and Kebara caves, Israel: macroscopic, microscopic, and mineralogical observations, and their archaeological implications. *Journal of Archaeological Science* 23, 763–781.

Schwarcz, H.P. and Rink, W.J. 1998. Progress in ESR and U-series chronology of the Levantine Paleolithic. In: *Neandertals and Modern Humans in Western Asia*, Akazawa, T., Aoki, K., and Bar-Yosef, O. (eds.). Plenum Press, New York, pp. 57–67.

Schwarcz, H. P., Buhay, W. M., Grün, R., Valladas, H., Tchernov, E., Bar-Yosef, O., and Vandermeersch, B. 1989. ESR dates of the Neanderthal site, Kebara Cave, Israel. *Journal of Archaeological Science* 16, 653–659.

Segev, A. and Sass, E. 2009a. *The Geology of the Carmel Region*. Report GSI/7/2009. Geological Survey of Israel, Jerusalem.

Segev, A. and Sass, E. 2009b. *Atlit, Sheet 3-III. Geological Map of Israel 1:50,000*. Geological Survey of Israel, Jerusalem.

Shahack-Gross, R., Ayalon, A., Goldberg, P., Goren, Y., Ofek, B., Rabinovitch, R., and Hovers, E. 2008. Formation processes of cemented features in karstic cave sites revealed using stable oxygen and carbon isotopic analyses: a case study at Middle Paleolithic Amud Cave, Israel. *Geoarchaeology* 23(1), 43–62.

Shahack-Gross, R., Berna, F., Karkanas, P., and Weiner, S. 2004. Bat guano and preservation of archaeological remains in cave sites. *Journal of Archaeological Science* 31, 1259–1272.

Shahack-Gross, R. and Ayalon, A. in press. Stable isotopes of carbon and oxygen in wood ash: an experimental study with archaeological implications. *Journal of Archaeological Science*.

Solecki, R.L. and Solecki, R.S. 1970. A new secondary flaking technique at the Nahr Ibrahim Cave site. *Bulletin du Musée de Beyrouth* 23, 137–142.

Stiner, M., Kuhn, S., Weiner, S., and Bar-Yosef, O. 1995. Differential burning, recrystallization, and fragmentation of archaeological bone. *Journal of Archaeological Science* 22, 223–237.

Tsartsidou, G., Lev-Yadun, S., Albert, R.M., Miller-Rosen, A., Efstratiou, N., and Weiner, S. 2007. The phytolith archaeological record: strengths and weaknesses evaluated based on a quantitative modern reference collection from Greece. *Journal of Archaeological Science* 34, 1262–1275.

Tsatskin, A. 2000. Acheulo-Yabrudian sediments of Tabun: a view from the microscope. In: *Toward Modern Humans—The Yabrudian and Micoqian 400–50 k-years Ago*, Ronen, A. and Weinstein-Evron, M. (eds.). BAR International Series 850, 133–143.

Valladas, H., Joron, J.-L., Valladas, G., Arensburg, B., Bar-Yosef, O., Belfer-Cohen, A., Goldberg, P., Laville, H., Meignen, L., Rak, Y., Tchernov, E., Tillier, A.-M., and Vandermeersch, B. 1987. Thermoluminescence dates for the Neanderthal burial site at Kebara in Israel. *Nature* 330, 159–160.

Valladas, H., Mercier, N., Hovers, E., Frojet, L., Joron, J.-L., Kimbel, W. H., and Rak, Y. 1999. TL dates for the Neandertal site of Amud Cave, Israel. *Journal of Archaeological Science* 26, 259–268.

Valladas, H., Mercier, N., Hershkovitz, I., Zaidner, Y., Vialetted, L., Joron, J-L., Reyss, J-L., and Weinstein-Evron, M. (in preparation). Thermoluminescence dating of burnt flints from Misliya Cave (Mount Carmel, Israel): new chronological data for the Levantine Early and Middle Paleolithic.

Villa, P. and Mahieu, E. 1991. Breakage patterns of human long bones. *Journal of Human Evolution* 21, 27–48.

Wadley, L., Sievers, C., Bamford, M., Goldberg, P., Berna, F., and Miller, C. 2011. Middle Stone Age bedding construction and settlement patterns at Sibudu, South Africa. *Science* 334, 1388–1391.

Weiner, S. 2010. *Microarchaeology: Beyond the Visible Archaeological Record*. Cambridge University Press, New York.

Weiner, S. and Bar-Yosef, O. 1990. States of preservation of bones from prehistoric sites in the Near East: a survey. *Journal of Archaeological Science* 17, 187–196.

Weiner, S., Goldberg, P., and Bar-Yosef, O. 1993. Bone preservation in Kebara Cave, Israel using on-site Fourier transform infrared spectrometry. *Journal of Archaeological Science* 20, 613–627.

Weiner, S., Schiegl S., Goldberg P., and Bar-Yosef O. 1995. Mineral assemblages in Kebara and Hayonim Caves, Israel: excavation strategies, bone preservation, and wood ash remnants. *Israel Journal of Chemistry* 35, 143–154.

Weiner, S., Goldberg, P., and Bar-Yosef, O. 2002. Three-dimensional distribution of minerals in the sediments of Hayonim Cave, Israel: diagenetic processes and archaeological implications. *Journal of Archaeological Science* 29, 1289–1308.

Weintein-Evron, M. and Tsatsakin, A. 1994. The Jamal Cave is not empty: recent excavations in the Mount Carmel Caves, Israel. *Paléorient* 20(2), 119–128.

Weintein-Evron, M. and Tsatsakin, A. 1995. Palaeoenvironmental investigations in the Jamal Cave, Mount Carmel, Israel. In: *Nature-Culture*, Otte M. (ed.). Liège, ERAUL 68, pp. 63–78.

Weinstein-Evron, M., Bar-Oz, G., Zaidner, Y., Tsatskin, A., Druck, D., Porat, N., and Hershkovitz, I. 2003a. Introducing Misliya Cave, Mount Carmel, Israel: a new continuous Lower/Middle Paleolithic sequence in the Levant. *Eurasian Prehistory* 1(1), 31–55.

Weinstein-Evron, M., Beck, A., and Ezersky, M. 2003b. Geophysical investigations in the service of Mount Carmel

prehistoric research. *Journal of Archaeological Science* 30, 1331–1341.

Weinstein-Evron, M. and Zaidner, Y. in preparation. Making a point: the Early Middle Paleolithic tool assemblage of Misliya Cave, Mount Carmel, Israel.

Wojtczak, D. 2011. Hummal (Central Syria) and its eponymous industry. In: The Lower and Middle Paleolithic in the Middle East and neighbouring regions, Le Tensorer, J.-M., Jagher, R., and Otte, M. (eds.). Liège, ERAUL 126, pp. 289–308.

Woodward, J.C. and Goldberg, P. 2001. The sedimentary records in Mediterranean rockshelters and caves: archives of environmental change. *Geoarchaeology* 16(4), 327–354.

Yaroshevich, A., Zaidner, Y., and Weinstein-Evron, M. in press. Projectile damage and point morphometry at the Early Middle Paleolithic Misliya Cave, Mount Carmel (Israel): preliminary results and interpretations. In: *Multidisciplinary Approaches to the Study of Stone Age Weaponry*, Iovita, R. and Sano, K. (eds.). Vertebrate Paleobiology and Paleoanthropology Series, Springer, Dordrecht.

Yeshurun, R., Bar-Oz, G., and Weinstein-Evron, M. 2007. Modern hunting behavior in the early Middle Paleolithic: faunal remains from Misliya Cave, Mount Carmel, Israel. *Journal of Human Evolution* 53, 656–677.

Zaidner, Y., Druck, D., Nadler, M., and Weinstein-Evron, M. 2005. The Acheulo-Yabrudian of Jamal Cave, Mount Carmel, Israel. *Journal of the Israel Prehistoric Society* 35, 93–116.

Zaidner, Y., Druck, D., and Weinstein-Evron, M. 2006. Acheulo-Yabrudian handaxes from Misliya Cave, Mount Carmel, Israel. In: *Axe Age: Acheulian Toolmaking—from Quarry to Discard*, Goren-Inbar, N. and Sharon, G. (eds.). Equinox Publishers, Oxford, pp. 243–266.